Author Manuscript

Author Manuscript

Author Manuscript

Author Manuscript

HHS Public Access

Author manuscript

Nat Microbiol. Author manuscript; available in PMC 2021 February 28.

Published in final edited form as:

Nat Microbiol. 2020 November ; 5(11): 1330–1339. doi:10.1038/s41564-020-0769-y.

LY6E impairs coronavirus fusion and confers immune control of viral disease

Stephanie Pfaender[1,2,3,#], **Katrina B. Mar**[4,#], **Eleftherios Michailidis**[5], **Annika Kratzel**[1,2,6], **Ian N. Boys**[4], **Philip V`kovski**[1,2], **Wenchun Fan**[4], **Jenna N. Kelly**[1,2], **Dagny Hirt**[1,2], **Nadine Ebert**[1,2], **Hanspeter Stalder**[1,2], **Hannah Kleine-Weber**[7,8], **Markus Hoffmann**[7], **H. Heinrich Hoffmann**[5], **Mohsan Saeed**[5,9], **Ronald Dijkman**[1,2,10,14], **Eike Steinmann**[3], **Mary Wight-Carter**[11], **Matthew B. McDougal**[4], **Natasha W. Hanners**[12], **Stefan Pöhlmann**[7,8], **Tom Gallagher**[13], **Daniel Todt**[3,14], **Gert Zimmer**[1,2], **Charles M. Rice**[5,*], **John W. Schoggins**[4,*], **Volker Thiel**[1,2,*]

[1]Institute of Virology and Immunology, Bern and Mittelhäusern, Switzerland. [2]Department of Infectious Diseases and Pathobiology, Vetsuisse Faculty, University of Bern, Bern, Switzerland. [3]Department for Molecular & Medical Virology, Ruhr-Universität Bochum, Germany. [4]Department of Microbiology, University of Texas Southwestern Medical Center, Dallas, TX, USA. [5]Laboratory of Virology and Infectious Disease, The Rockefeller University, New York, NY, USA. [6]Graduate School for Cellular and Biomedical Sciences, University of Bern, Bern, Switzerland. [7]Deutsches Primatenzentrum GmbH, Leibniz-Institut für Primatenforschung, Göttingen, Germany. [8]Faculty of Biology and Psychology, University Göttingen, Göttingen, Germany. [9]Department of Biochemistry, Boston University School of Medicine, Boston, MA, USA; National Emerging Infectious Diseases Laboratories, Boston University, Boston, MA, USA. [10]Institute for Infectious Diseases, University of Bern, Bern, Switzerland. [11]Animal Resource Center, University of Texas Southwestern Medical Center, Dallas, TX, USA. [12]Department of Pediatrics, University of Texas Southwestern Medical Center, Dallas, TX, USA [13]Department of Microbiology and Immunology, Loyola University Chicago, Chicago, USA. [14]European Virus Bioinformatics Center (EVBC), Jena, Germany

Abstract

Users may view, print, copy, and download text and data-mine the content in such documents, for the purposes of academic research, subject always to the full Conditions of use:http://www.nature.com/authors/editorial_policies/license.html#terms

Materials & Correspondence Correspondence and requests for materials should be addressed to Volker Thiel, John W. Schoggins, or Charles M. Rice., volker.thiel@vetsuisse.unibe.ch, john.schoggins@utsouthwestern.edu, ricec@rockefeller.edu.

[#]equally contributing authors

[*]equal senior authorship

Author contributions

S.P., K.B.M., E.M., C.M.R., J.W.S., and V.T. designed the project. S.P., K.B.M., E.M., A.K., I.N.B., P.V., W.F., D.H., N.E., H.S., H.K-W., M.H., H.H.H., M.S., M.B.M., and G.Z. performed and analyzed *in vitro* experiments. K.B.M. performed and analyzed *in vivo* experiments with assistance from W.F. and N.W.H.. M. W-C. performed histological analysis. D.T. performed statistical analysis and analysis of MHV RNA-seq dataset. J.N.K. performed statistical analysis and analysis of hAEC RNA-seq dataset. R.D., S.Pö., E.S., and T.G. contributed to the design and implementation of the research. S.P., K.B.M., and J.W.S. wrote the manuscript, and all authors contributed to editing.

Competing interest declaration

The authors declare no competing interests.

Supplementary Information is available for this paper.

Author Manuscript Author Manuscript Author Manuscript Author Manuscript

Zoonotic coronaviruses (CoVs) are significant threats to global health, as exemplified by the emergence of two severe acute respiratory syndrome CoVs (SARS-CoV and SARS-CoV-2) and Middle East respiratory syndrome CoV (MERS-CoV) within two decades[1–3]. Host immune responses to CoVs are complex and regulated in part through antiviral interferons. However, interferon-stimulated gene products that inhibit CoVs are not well characterized4. Here, we show that lymphocyte antigen 6 complex, locus E (LY6E) potently restricts infection by multiple CoVs, including SARS-CoV, SARS-CoV-2, and MERS-CoV. Mechanistic studies revealed that LY6E inhibits CoV entry into cells by interfering with spike protein-mediated membrane fusion. Importantly, mice lacking Ly6e in hematopoietic cells were highly susceptible to a murine CoV, mouse hepatitis virus. Exacerbated viral pathogenesis in Ly6e knockout mice was accompanied by loss of hepatic immune cells, higher splenic viral burden, and reduction in global antiviral gene pathways. Accordingly, we found that constitutive Ly6e directly protects primary B cells from murine CoV infection. Our results demonstrate that LY6E is a critical antiviral immune effector that controls CoV infection and pathogenesis. These findings advance our understanding of immune-mediated control of CoV *in vitro* and *in vivo*, knowledge that could help inform strategies to combat infection by emerging CoVs.

Coronaviruses (CoVs) are enveloped RNA viruses with broad host tropism and documented capability to cross the species barrier to infect humans[5]. The mammalian innate immune response controls CoV infection partly through the action of interferons (IFNs)[4,6,7]. IFNs inhibit viral infection by inducing hundreds of genes, many of which encode antiviral effectors[8]. The interferon-stimulated genes (ISGs) that inhibit CoV infection are not well defined[4]. To address this knowledge gap, we screened our published library of >350 human ISG cDNAs[9,10] in human hepatoma cells for antiviral activity against the endemic human CoV 229E (HCoV-229E) (Supplementary Table 1, Supplementary Table 2). The ISG lymphocyte antigen 6 complex, locus E (LY6E) strikingly inhibited HCoV-229E infection (Fig. 1a–b, Extended Data Fig. 1a). This was unexpected since we and others previously reported that LY6E enhances cellular infection by influenza A virus, flaviviruses, and HIV-1[11–13], with HIV-1 being an exception with opposing roles of LY6E described[14]. To verify this result, we generated stable cell lines ectopically expressing LY6E and infected cells with diverse CoVs. In addition to HCoV-229E (Fig. 1c), LY6E significantly reduced infection by HCoV-OC43 (Fig. 1d), MERS-CoV (Fig. 1e), SARS-CoV (Fig. 1f), and the recently emerged SARS-CoV-2 (Fig. 1g, Extended Data Fig. 1b). The antiviral effect of LY6E extended beyond human CoVs and decreased infection by the murine CoV mouse hepatitis virus (MHV) (Fig. 1h). Given the zoonotic origin of MERS-CoV, SARS-CoV and SARS-CoV-2, all suspected to originate from bats, we next tested the antiviral potential of select LY6E orthologues. All LY6E orthologues inhibited HCoV-229E (Extended Data Fig. 1c). Recent surveillance of Kenyan camels, the main viral reservoir for MERS-CoV, indicates active circulation of the zoonotic CoV[13]. Human and camel LY6E restricted MERS-CoV infection (Extended Data Fig. 1d). To confirm the presence of LY6E in respiratory cells that are targeted by HCoV, we examined expression in primary human airway epithelial cells (hAEC) by single cell RNA-seq (scRNA-seq). LY6E was widely expressed in all cell types, with the greatest levels observed in goblet cells (Fig. 1i). We additionally assessed expression of known HCoV receptors in hAEC by scRNA-seq and observed broad expression of the HCoV-229E receptor *CD13*, the MERS-CoV receptor

Author Manuscript Author Manuscript Author Manuscript Author Manuscript

DPP4, and the SARS-CoV and SARS-CoV-2 receptor *ACE2* in multiple cell types (Extended Data Fig. 1e–g). Infection of hAEC with SARS-CoV-2, but not SARS-CoV, potently induced expression of LY6E in hAEC at 3 days post-infection (Fig. 1j). LY6E has been previously shown to restrict HIV-1 infection by promoting internalization of the receptor CD4[14]. When we ectopically expressed ACE2 in human hepatoma cells, SARS-CoV-2 infectivity increased, but LY6E still restricted SARS-CoV-2. (Fig. 1k–l, Extended Data Fig. 1h). Importantly, total levels of ectopically expressed ACE2 were unaltered by LY6E expression (Extended Data Fig. 1i). Furthermore, LY6E expression had no effect on cell surface levels of other CoV receptors CD13 (Extended Data Fig. 1j) or DPP4 (Extended Data Fig. 1k). Collectively, our data shows that LY6E is a constitutively-expressed ISG that restricts infection by endemic and pandemic CoVs without modulating expression of viral receptors.

To test the role of endogenous LY6E in controlling CoV infections, we used CRISPR-Cas9 gene editing to ablate LY6E expression in human lung adenocarcinoma cells (Fig. 1m). This cell line was selected as human hepatoma cells do not express LY6E irrespective of IFN treatment[11]. LY6E knockout (KO) cells were more susceptible to HCoV-229E (Fig. 1n). Reconstitution with a CRISPR-resistant *LY6E* variant (*CR LY6E*) restored antiviral activity in KO cells (Fig. 1o–p). Strikingly, the LY6E-mediated restriction in hepatoma cells was largely specific to CoVs. Among 10 genetically divergent viruses tested, only hepatitis C virus was also restricted (Extended Data Fig. 1l).

LY6E is a member of the LY6/uPAR family of GPI-anchored proteins, and is implicated in diverse cellular processes[15]. To evaluate the specificity of LY6E for inhibiting CoVs, we ectopically expressed selected LY6/uPAR proteins[11] and infected with HCoV-229E. Only LY6E inhibited CoV infection (Extended Data Fig. 1m). We previously showed that a conserved residue (L36) is required for LY6E-mediated enhancement of influenza A virus[11]. L36 was also required to restrict HCoV-229E infection (Extended Data Fig. 1n). These data suggest a conserved functional domain that is responsible for both the virus-enhancing and -restricting phenotypes.

Next, we investigated the effect of LY6E on specific steps of the virus replication cycle. First, we tested whether LY6E restricts CoV attachment to the cell surface and observed no effect on HCoV-229E binding (Extended Data Fig. 2a). To test whether LY6E restricts viral entry, we used a vesicular stomatitis virus (VSV) pseudoparticle (pp) system bearing CoV spike (S) proteins. Strikingly, LY6E significantly inhibited VSVpp entry mediated by S proteins from HCoV-229E (Fig. 2a), MERS-CoV (Fig. 2a), SARS-CoV (Fig. 2b), and SARS-CoV-2 (Fig. 2b). Entry mediated by VSV glycoprotein G was not affected by LY6E (Fig. 2a–b). Time-course experiments revealed that LY6E had no effect on CoV translation, replication, assembly, or release as assessed with HCoV-229E (Extended Data Fig. 2b–f). To further narrow down the entry phenotype, we tested whether LY6E interferes with the fusion of viral and cellular membranes. To this end, we performed a syncytia formation assay using propagation competent VSV pseudoviruses co-expressing CoV S protein and a GFP reporter (VSV*ΔG(CoV S)) (Extended Data Fig. 3a). LY6E potently inhibited CoV S protein-mediated syncytia formation (Fig. 2c–d). To determine whether LY6E impairs S protein expression or maturation, we also performed a heterologous syncytia formation assay. CoV-

Author Manuscript Author Manuscript Author Manuscript Author Manuscript

resistant hamster cells infected with trans-complemented GFP reporter VSV*ΔG(CoV) were co-cultured with susceptible target cells that ectopically expressed LY6E. LY6E again significantly blocked syncytia formation, demonstrating that LY6E inhibits S protein-mediated fusion and not S protein expression or maturation (Extended Data Fig. 3b–c). As membrane fusion can occur without syncytia formation, we also performed a quantitative fusion assay in which mixing of cell contents results in complementation of split-luciferase/split-GFP (Fig. 2e–h). Cells co-transfected with plasmids encoding CoV S proteins and split-GFP were mixed with susceptible target cells co-expressing LY6E or vector control and the complementary fragment of split-GFP. LY6E reduced CoV S-mediated cell-cell fusion of HCoV-229E (Fig. 2e–f), MERS-CoV (Fig. 2e–f), and SARS-CoV-2 (Fig. 2g–h) as visualized by reduction of GFP-positive syncytia, indicating that LY6E blocks fusion of viral and cellular membranes. Importantly, no effect on control cells (mCherry-transfected or VSV-G) could be observed (Fig. 2e–h). SARS-CoV did not induce cell-cell fusion in this experimental setup, consistent with recent observations (Fig. 2g–h)[16,17]. Collectively, our results demonstrate that LY6E specifically inhibits CoV S protein-mediated membrane fusion, which is required for productive viral entry.

We next addressed whether LY6E influences proteolytic activation of the S protein. After S protein-mediated binding to the respective receptor, host proteases cleave the S protein, activating membrane fusion[18] at cell surfaces or within endosomes[19]. Inhibitors of cell surface and endosomal proteases suppressed infection but had no effect on LY6E-mediated restriction of CoV infection (Extended Data Fig. 4a–c). Proteolytic activation is also suppressed by cleavage site mutations[19,20]. Mutation of S1/S2 and S2′ in the S protein of MERS-CoV reduced activation (Extended Data Fig. 4d)[19,20]. LY6E overexpression did not affect S1/S2 cleavage (Extended Data Fig. 4e–f) and did not affect the level of mutant MERS-CoV S pp cell entry (Extended Data Fig. 4g). Collectively, our data indicate that restriction of viral fusion is independent of S protein activation.

Next, we aimed to evaluate LY6E-mediated CoV restriction *in vivo*. Systemic genetic ablation of *Ly6e* in mice is embryonic lethal[21]. Therefore, we generated transgenic $Ly6e^{fl/fl}$ mice, which are functionally ‘wild-type (WT)’ for Ly6e expression, and crossed them with *Vav1-iCre* mice to ablate *Ly6e* in cells that originate from a hematopoietic stem cell (HSC) progenitor (Extended Data Fig. 5a–b). This genetic model was chosen since immune cells are critical for protection from CoVs *in vivo*[7,22–26]. Bone-marrow derived macrophages (BMDM) from $Ly6e^{\Delta HSC}$ mice had reduced *Ly6e* mRNA levels (Extended Data Fig. 5c). The natural mouse pathogen MHV is a well-studied model CoV that causes hepatitis and encephalomyelitis in mice[27]. $Ly6e^{\Delta HSC}$ BMDM were more susceptible to MHV infection than $Ly6e^{fl/fl}$ BMDM, demonstrating that murine Ly6e is a restriction factor for murine CoV (Extended Data Fig. 5d).

To determine whether Ly6e is important for controlling CoV infection *in vivo*, $Ly6e^{fl/fl}$ and $Ly6e^{\Delta HSC}$ mice were infected with a high dose (5×10^4 PFU) of MHV that causes sub-lethal hepatitis in WT C57BL/6J mice[28]. Since MHV pathogenesis is influenced by sex, with higher levels of viral replication and hepatic damage observed in male mice[29], we performed independent experiments in male and female mice. $Ly6e^{\Delta HSC}$ mice of both sexes rapidly succumbed to MHV infection by day 6 (Fig. 3a–b, Extended Data Fig. 6a–b). To examine

Author Manuscript Author Manuscript Author Manuscript Author Manuscript

viral pathogenesis and immunopathology in infected mice, *Ly6e*$^{fl/fl}$ and *Ly6e*$^{\Delta HSC}$ mice were infected with the same high dose of MHV and euthanized 3- or 5-days post-infection. At both time points, female *Ly6e*$^{\Delta HSC}$ mice exhibited significantly higher levels of liver damage as measured by serum ALT while no difference was observed in male mice (Fig. 3c,i, Extended Data Fig. 6c,i). However, hepatic viral burden did not differ in either sex (Fig. 3d,j, Extended Data Fig. 6d,j), possibly due to tissue saturation at this high dose. At a lower dose of MHV (5 PFU), viral burden and liver damage was elevated in female mice, but not in male mice which exhibited saturated hepatic infection, likely due to increased susceptibility as previously reported (Extended Data Fig. 7a–b, f–g)[29]. Spleen viral burden was elevated in female and male *Ly6e*$^{\Delta HSC}$ mice at both time points and doses of MHV (Fig. 3e,k, Extended Data Fig. 6e,k, Extended Data Fig. 7c,h). At 3 days post-infection, there was no difference in liver necrosis, but inflammation was moderately reduced in female but not male *Ly6e*$^{\Delta HSC}$ mice (Fig. 3f–h, Extended Data Fig. 6f–h). By 5 days post-infection and at both low and high doses of MHV, female *Ly6e*$^{\Delta HSC}$ mice had significantly higher levels of liver necrosis and a reduced presence of mononuclear immune cells (Fig. 3l–n, Extended Data Fig. 7d–e), whereas no difference was observed in male mice (Extended Data Fig. 6l–n, Extended Data Fig. 7i–j). Liver damage in *Ly6e*$^{\Delta HSC}$ mice was further corroborated at an intermediate viral dose (5×10^3 PFU), which resulted in visibly apparent brittleness, pallor, and necrotic foci (Extended Data Fig. 7k–n). These data demonstrate that Ly6e in hematopoietic cells is important for controlling murine CoV infection.

We next used a transcriptomic approach to evaluate the effect of *Ly6e* ablation on global gene expression in liver and spleen of female *Ly6e*$^{fl/fl}$ and *Ly6e*$^{\Delta HSC}$ mice injected with PBS or the high dose of MHV at 3- and 5- days post-infection. In infected tissues, loss of *Ly6e* in hematopoietic cells correlated with differential gene expression in pathways associated with tissue damage, such as liver-specific metabolic genes, angiogenesis, wound healing, and immune response to viruses (Fig. 4a–c). We also observed a striking loss of genes associated with the type I IFN response, inflammation, antigen presentation, and B cells in livers and spleens from infected *Ly6e*$^{\Delta HSC}$ mice (Extended Data Fig. 7o–p, Extended Data Fig. 8).

The histopathology (Fig. 3h,n) and transcriptome data (Fig 4a–c, Extended Data Fig. 7o–p, Extended Data Fig. 8) prompted us to determine how loss of *Ly6e* affects immune cell numbers during infection. Absolute numbers of different immune cell subsets were quantified in spleen and liver from female and male *Ly6e*$^{\Delta HSC}$ and *Ly6e*$^{fl/fl}$ mice 5 days after injection with PBS or the intermediate dose of MHV (Extended Data Fig. 9). In infected male mice, hematopoietic *Ly6e* protected hepatic B cells, recruited NK cells, dendritic cells (DC), macrophages, and neutrophils, but had no influence on $CD8^+$ T cell recruitment (Extended Data Fig. 10a). Hematopoietic *Ly6e* in infected female mice protected hepatic B cells and $CD4^+$ T cells as well as recruited NK cells (Fig. 4d). Multiple splenic cell populations were also altered with MHV infection in both male and female mice (Fig. 4e, Extended Data Fig. 10b). Depletion of immune cell populations in *Ly6e*$^{\Delta HSC}$ organs was MHV-dependent, as cell numbers were similar between PBS-injected *Ly6e*$^{\Delta HSC}$ and *Ly6e*$^{fl/fl}$ mice of both sexes.

To determine whether loss of immune cells in MHV-infected *Ly6e*$^{\Delta HSC}$ mice correlates with increased permissiveness to infection, we assessed MHV infection in splenocytes cultured

Author Manuscript Author Manuscript Author Manuscript Author Manuscript

from *Ly6e*$^{\Delta HSC}$, *Ly6e*$^{fl/fl}$, and *Ifnar*$^{-/-}$ mice. In *Ly6e*$^{fl/fl}$ splenocyte cultures, MHV infected macrophages, neutrophils, DC, and B cells, but not CD4$^+$ or CD8$^+$ T cells, as previously reported (Fig. 4f–g)[26]. Strikingly, B cells from both male and female *Ly6e*$^{\Delta HSC}$ mice were highly susceptible to MHV infection when compared to B cells from *Ly6e* $^{fl/fl}$ mice (Fig. 4h–i). Antiviral protection from MHV was likely conferred by constitutive *Ly6e* expression, as B cells from *Ifnar*$^{-/-}$ mice showed similar resistance to MHV as cells from *Ly6e* $^{fl/fl}$ mice. In female mice, only neutrophils from *Ly6e*$^{\Delta HSC}$ mice were more susceptible to MHV infection when compared to cells from *Ifnar*$^{-/-}$ but not *Ly6e* $^{fl/fl}$ mice (Extended Data Fig. 10c). DC and macrophages from male *Ly6e*$^{\Delta HSC}$ mice were also more susceptible to MHV infection than respective cells from *Ly6e*$^{fl/fl}$ mice (Extended Data Fig. 10d). Surprisingly, no other cell type demonstrated a strong Ly6e-dependent susceptibility to MHV infection.

Together, our data demonstrate an important role for Ly6e in immune cell-mediated control of CoV infection. Our observation of higher splenic viral burden and infection-associated alterations in hepatic and splenic cellular subsets indicate that mortality may be due to viral pathogenesis that exceeds the ability of the immune system to control the infection. Notably, we observed MHV-induced loss of three classes of cells in *Ly6e*$^{\Delta HSC}$ mice: 1) cells that are not permissive to the virus (CD4$^+$ T cells), 2) cells that are permissive to MHV but do not demonstrate *Ly6e* KO-dependent infection (NK cells), and 3) cells that are permissive to MHV in a *Ly6e* KO-dependent manner (B cells, neutrophils, macrophages, and DC). The increased susceptibility and reduction of *Ly6e*-deficient B cells suggest that the lymphocytes may be key for restricting MHV replication and may possibly participate in downstream immune responses.

In conclusion, we identified LY6E as a CoV restriction factor that limits CoV entry and protects the host from severe viral disease. Our findings are striking given that LY6E has been primarily associated with an enhancing phenotype in which LY6E promotes entry of multiple viruses[11–13]. However, our data clearly expand the role of LY6E during coronaviral infection and establish a novel function in protecting the host immune cell compartment. Determining the precise molecular mechanism underlying how LY6E inhibits CoV S protein-mediated membrane fusion will advance our understanding of cellular antiviral defenses against these important human pathogens. Antiviral membrane fusion inhibitors have been successfully implemented for treatment of HIV-1 infection[30]. A therapeutic approach mimicking the mechanism of action of LY6E could provide a first line of defense against novel emerging CoV infections. Furthermore, additional *in vivo* work will be needed to delineate which Ly6e-expressing immune cells protect mice from MHV, and for assessing the role of Ly6e during the pathogenesis of medically-relevant human coronaviruses such as SARS-CoV, MERS-CoV, and SARS-CoV-2.

Methods

Viral infection assays

HCoV-229E: 1.5×10^5 stable LY6E expressing or control cells were seeded in a 12-well plate and infected with HCoV-229E in a serial dilution. Cells were incubated for 2 hours at 33°C, then viral supernatant was removed, and an overlay of 1:1 Avicel (2.4%) (Avicel RC-581NF) and 2x DMEM, supplemented with 10% FBS and 100 IU/ml penicillin

Author Manuscript Author Manuscript Author Manuscript Author Manuscript

(Gibco)/100 μg/ml streptomycin (Gibco) (p-s), was added. Cells were incubated for 3 days at 33°C before medium was removed, cells were washed, and stained with crystal violet (Sigma-Aldrich). Plaque forming units (PFU) were calculated.

HCoV-OC43: 5.0×10^4 stable LY6E expressing or control cells were seeded in a 24-well plate and infected at 33°C for 1 hour with HCoV-OC43 (MOI=1). Virus was aspirated and 10% FBS/1x NEAA/1x p-s/RPMI (cRPMI) was added back to cells. 24 hours post-infection, cells were dissociated using Accumax (Sigma-Aldrich), fixed in 1% PFA, permeabilized per manufacturer's protocol (BD Cytofix/Cytoperm), and stained for nucleoprotein (1:500) and a goat anti-mouse AlexaFluor488-conjugated secondary antibody (1:2000). Infection was analyzed by flow cytometry.

MERS-CoV/ SARS-CoV/ SARS-CoV-2: 1×10^4 stable LY6E expressing or control cells were seeded in a 96-well plate and infected at 37°C in a serial dilution assay. 3–4 days post-infection supernatant was removed, and cells were stained with crystal violet (Sigma-Aldrich). Cytopathic effect (CPE) was determined upon visual inspection and $TCID_{50}$/ml calculated according to the Reed and Muench method.

SARS-CoV-2 infection in Huh7.5: 5×10^4 stable LY6E expressing or control cells were seeded in a 24-well plate and infected at 37°C for 1 hour. At 24 hours post-infection, cells were harvested, permeabilized, and analyzed as described for HCoV-OC43 with the exception of 4% PFA for fixation and staining for dsRNA (1:10,000) and a goat anti-mouse AlexaFluor488-conjugated secondary antibody (1:1000).

MHV-Gluc: 1×10^5 stable LY6E expressing or control cells were seeded in a 24-well plate and infected with MHV-Gluc (MOI=0.1) at 37°C. After 2 hours, virus inoculum was removed, cells were washed with PBS, and cRPMI added back. 24 hours post-infection, cell culture supernatant was harvested, and Gluc activity was measured using Pierce Gaussia Luciferase Glow Assay Kit (ThermoFisher Scientific) and a plate luminometer (EnSpire 2300 Multilabel reader by Perkin Elmer). For testing the virus panel against LY6E, 1×10^4 stable LY6E expressing or control Huh7.5 cells were seeded in a 96-well plate. Cells were infected with the following viruses and harvested after the indicated time: HCoV-229E (MOI=0.001, 72 hours), HCV-Ypet (MOI=1, 72 hours), CHIKV-GFP (MOI=0.005, 24 hours), hPIV-3-GFP (MOI=0.015, 24 hours), RSV-GFP (MOI=1.5, 24 hours), SINV-GFP (MOI=0.1, 24 hours), VEEV-GFP (MOI=0.0075, 24 hours), WNV-GFP (MOI=1.5, 24 hours), ZIKV PRVABC59 (MOI=0.01, 48 hours), YFV 17D-venus (MOI=0.01, 48 hours) and DENV-GFP (MOI=0.05, 72 hours). At the indicated time points, cells were fixed with 4% paraformaldehyde (PFA)/PBS. ZIKV-infected cells were stained for viral E protein (1:500) and an AlexaFluor488-conjugated goat anti-mouse secondary antibody (1:1000). Images were acquired with a fluorescence microscope and analyzed using ImageXpress Micro XLS (Molecular Devices, Sunnyvale, CA).

SARS-CoV-2 infection of ACE2-expressing cells

Approximately 3×10^4 Huh7.5 were plated in 8 well chamber slides. Cells were infected in a low volume with 0.5 MOI SARS-CoV-2 for 1 hour at 37°C, incubated for 9 more hours at full volume, and then fixed in 3.7% formaldehyde. Cells were permeabilized, stained for

Author Manuscript Author Manuscript Author Manuscript Author Manuscript

dsRNA (1:500, see 'Antibodies for immunofluorescence and flow cytometry'), and imaged as previously described, except mounting was performed with Vectashield with DAPI (Cat #H-1200, Vector Labs)[31]. Seven images were acquired for each condition. Images were processed using ImageJ by equally adjusting minimum brightness to normalize background and measuring the mean intensity of the entire dsRNA image. Nuclei were enumerated using ImageJ by using the threshold, watershed, and analyze particles feature. MFI/nuclei was determined by dividing the mean intensity of the GFP channel by number of total nuclei in the field.

HCoV-229E-Rluc infection assay of KO cells

For infection assays, 1×10^5 target cells were seeded in a 24-well plate one day prior infection. Cells were infected with HCoV-229E-Rluc (MOI 0.1) in OptiMEM (Gibco) for 2 hours at 33°C. Cells were washed 1x with PBS and 10% FBS/1x NEAA/1x p-s/DMEM (cDMEM) was added back. Cells were incubated at 33°C for 24 hours, then washed with PBS and lysed using the Renilla Luciferase Assay System kit (Promega). Rluc activity was measured using a plate luminometer (EnSpire 2300 Multilabel reader by Perkin Elmer). For the reconstitution with CRISPR resistant LY6E (CR LY6E), 2.5×10^4 cells were seeded in a 24-well plate. One day post-seeding, cells were either left untransduced or transduced with a lentiviral vector encoding for CR LY6E or the empty control. 48 hours post-transduction, cell lysates were either infected with HCoV-229E-Rluc (MOI=0.1) for 24 hours as described above or harvested for Western blot.

VSV pseudoparticles

Pseudotyping of VSV*ΔG(Fluc) was performed as previously described[32]. Briefly, 6×10^5 293LTV cells were seeded in a 6-well plate and transfected using Lipofectamine 2000 (Invitrogen) which was complexed with DNA plasmids driving the expression of either VSV G protein (positive control), the respective CoV S proteins, or the fluorophore mCherry (negative control). Expression vectors for vesicular stomatitis virus (VSV, serotype Indiana) glycoprotein (VSV-G, Genbank accession number: NC_001560), HCoV-229E S (pCAGGS-229E S, Genbank accession number: X16816), MERS-CoV S (pCAGGS-MERS S, Genbank accession number: JX869059 with silent point mutation (C4035A, removing internal XhoI), SARS-CoV S (pCAGGS-SARS S, Genbank accession number: AY291315.1 with two silent mutation (T2568G, T3327C)), have been described previously[33,34]. The expression plasmid for SARS-CoV-2 was generated as follows: the coding sequence of a synthetic, codon-optimized (for human cells) SARS-CoV-2 DNA (GeneArt Gene Synthesis, Thermo Fisher Scientific) based on the publicly available protein sequence in the National Center for Biotechnology Information database (NCBI Reference Sequence: YP_009724390.1) was PCR-amplified and cloned into the pCG1 expression vector between BamHI and XbaI restriction sites. The MERS-CoV S cleavage mutants have been described before[20]. pCAGGS_mCherry was generated upon cloning of the mCherry reporter gene into the pCAGGS expression vector (primer sequences and cloning procedure are available upon request). At 20 hours post-transfection, cells were infected with VSV-G-trans-complemented VSV*ΔG(FLuc) (MOI=5) for 30 minutes at 37°C, washed with PBS, and further incubated for 1 hour in cDMEM that was supplemented with Mab I1 (ATCC, 1:100), a neutralizing monoclonal antibody directed to the VSV G protein. Cells were then washed and cDMEM

Author Manuscript Author Manuscript Author Manuscript Author Manuscript

was added back. Viral supernatant was harvested at 16 – 24 hours post-infection. Cellular debris was removed by centrifugation (3,000 × *g* for 10 minutes) and used to inoculate 2 × 10^4 target cells in a 96-well plate (6 technical replicates). Cells were incubated for 16–18 hours at 37°C before Fluc activity in cell lysates was detected using a plate luminometer (EnSpire 2300 Multilabel reader by Perkin Elmer) and the Bright-Glo Luciferase Assays System (Promega). Experiments with pseudotyped SARS-CoV and SARS-CoV-2 were performed as previously described[20].

Cell-cell fusion assay

The cell-cell luciferase/GFP fusion assay has been described before, with slight modifications[35]. Briefly, 6 × 10^5 293LTV cells were transfected with plasmids encoding CoV S proteins (for the constructs please refer to VSV pseudoparticles; pCAGGS-HCoV-229E, pCAGGS-MERS-CoV, pCAGGS-SARS-CoV, pCAGGS-SARS-CoV-2) together with a split-luciferase/split-GFP construct (Rluc8155–156 DSP1–7). The empty expression plasmid (pCAGGS-mCherry) as well as a construct encoding for VSV-G served as negative and positive control, respectively. 2 × 10^5 stable LY6E expressing or empty control Huh7 or VeroE6 cells were transfected using Lipofectamine 2000 (Thermo Fisher Scientific) with a plasmid encoding the complementary fragment of the split-luciferase/split-GFP protein (Rluc8155–156 DSP8–11). Approximately 30 hours post-transfection, both cell populations were dissociated (TryPLE Express, Gibco), counted, and equal cell numbers (2 × 10^4 cells each) were co-cultured for 16 – 20 hours at 37°C. Cells were rinsed with PBS and fixed using 4% PFA in PBS. Four images were acquired using a EVOS FL Auto 2 imaging system equipped with a 4x air objective (NA=0.13) and stitched using the integrated software (ImageJ 2.0.0-rc-69/1.52p; Java 1.8.0_172 [64-bit]; Windows 10 10.0). Images were processed by applying background subtraction (rolling ball, size = 25 pixels) and measuring the mean intensity of the entire image.

Syncytia formation assay

Cells expressing LY6E or empty control were infected with VSV*ΔG(MERS S) or VSV*ΔG(229E S) at a MOI of 0.01. At 20 hours post-infection, the cells were fixed with 3% PFA/PBS and the nuclei stained with 4’,6-diamidine-2’-phenylindole (DAPI, Sigma, 1:10,000). An inverted fluorescence microscope (Zeiss) was used to determine area percentage area covered by syncytia.

For heterologous cell-cell fusion assay, BHK-21 cells were infected with VSV*ΔG(CoV S) at a MOI of 1. After 2 hours, the cells were treated with trypsin/EDTA (Life Technologies, Zug, Switzerland) and resuspended in DMEM supplemented with 5% FBS (2×10^4 cells/mL). The infected BHK-21 cell suspension (500 µL) was seeded into 24-well cell culture plates along with LY6E- or empty control-expressing Huh7 (1 × 10^4 cells). Cell co-cultures were incubated for 7 hours at 37°C, fixed with 3.6% formaldehyde diluted in PBS, (Grogg-Chemie AG, Stettlen, Switzerland) and stained with DAPI. The percentage area covered by syncytia was calculated as above.

Author Manuscript Author Manuscript Author Manuscript Author Manuscript

Mice

Ly6e^{tm1a} ES cells were obtained from the EUCOMM consortium[36] and microinjected into C57BL/6J blastocysts by the UTSW Transgenic Technology Center. Chimeric mice with germline transmission were bred to obtain *Ly6e*$^{tm1a/+}$ offspring. *Ly6e*$^{tm1a/+}$ mice were crossed with FLPe-expressing mice (*B6N.129S4-Gt(ROSA)26Sor*$^{tm1(FLP1)Dyn}$*/J, #*16226, Jackson Laboratories) to obtain *Ly6e*$^{fl/+}$ offspring, which were bred to homozygosity. Conditional *Ly6e*$^{fl/fl}$ mice were bred to *Vav1-iCre* transgenic mice (B6.Cg-Commd10$^{Tg(Vav1-icre)A2Kio}$/J, #008610, Jackson Laboratories) to obtain *Ly6e*$^{\Delta HSC/+}$ (*Ly6e*$^{fl/+}$*; Vav1-iCre*) offspring. *Ly6e*$^{\Delta HSC/+}$ mice were bred to obtain *Ly6e*$^{\Delta HSC}$ (*Ly6e*$^{fl/fl}$*; Vav1-iCre*) offspring, which harbor a deletion of exon 3 and 4 in hematopoietic stem cells (HSC). Experimental animals were obtained by crossing *Ly6e*$^{\Delta HSC}$ and *Ly6e*$^{fl/fl}$ mice. Littermates were used for the majority of experiments when possible; otherwise mice of similar age (within 2 weeks) were used. Sample size was chosen based on published studies and no randomization or blinding was performed aside from scoring of liver histology. Genotype was confirmed by PCR of genomic DNA in-house or outsourced to Transnetyx. Ablation of *Ly6e* was confirmed by qPCR in immune cells from spleen, liver, or bone marrow. *Ifnar*$^{-/-}$ mice on a C57BL/6J background were a kind gift from N. Yan (UTSW). Animal studies were carried out in specific-pathogen-free barrier facilities managed and maintained by the UTSW Animal Resource Center. Facilities are maintained at an acceptable range of 68–79°F at a humidity of 30–70% on a 12 hour dark/12 hour light cycle. All procedures used in this study complied with federal and institutional guidelines enforced by the UTSW Institutional Animal Care and Use Committee (IACUC) and were granted institutional approval after veterinary and committee review.

In vivo infection, viral titers, liver ALT, and liver histology

Six to twelve-week-old female and male mice were injected intraperitoneally with MHV-A59 diluted in PBS to the indicated titers or PBS for a mock infection control. Unless otherwise indicated, *Ly6e*$^{fl/fl}$ mice were used for mock infection controls. All infected mice were monitored daily for weight and mortality. Animals that lost more than 20% of their original body weight were euthanized per IACUC guidelines.

Viral titers in liver and spleen were determined from frozen organs after weighing, homogenization, and plaque assay on L929 cells. Alanine aminotransferase (ALT) was measured in fresh, unfrozen serum using VITROS MicroSlide Technology by the UTSW Mouse Metabolic Core. Livers were fixed in 10% neutral buffer formalin, embedded in paraffin, sectioned at 5 μM, and stained with hematoxylin and eosin (H&E). Slides were analyzed by an independent pathologist (UTSW Animal Resource Center) who was blinded to experimental conditions. A numerical score was assigned for degree of inflammation and degree of necrosis for each liver. Inflammatory cell infiltration was scored using the following criteria: 0 = none, 1 = minimal, 2 = mild, 3 = moderate, and 4 = marked. The necrosis score was defined by the percent necrosis. 0 = none, 1 = <2%, 2 = 2–20%, 3 = 21–40%, and 4 = >40%.

Author Manuscript Author Manuscript Author Manuscript Author Manuscript

Primary cell preparation for flow cytometry

Primary cells were isolated from six to fifteen-week-old female and male mice. All primary cells were maintained in 10% FBS/10 mM HEPES/1 mM sodium pyruvate/2 mM L-glutamine/1x p-s/RPMI (cRPMI2) unless otherwise indicated.

Primary bone marrow derived macrophages (BMDM) were prepared as described previously[37]. Viable cells were quantified using trypan blue exclusion. BMDM were plated at 2.5×10^4 cells per well in non-treated 24-well tissue culture plates. Cells were infected the next day with MOI 0.1 of MHV-A59-GFP and isolated 6 hours post-infection for analysis by flow cytometry.

Splenocytes were prepared by mashing whole spleens against a 70 μM cell strainer. Red blood cells were removed by using RBC lysis buffer (Tonbo Biosciences). Viable cells were quantified using trypan blue exclusion. For *in vitro* infection, splenocytes were plated at $1{\times}10^6$ cells per well in non-treated 6-well tissue culture plates and immediately infected with MOI 1 of MHV-A59-GFP for 2 hours before increasing media volume 5-fold. Infected cells were isolated 8 hours post-infection, stained with a fluorescent viability dye (Ghost Dye Violet 450, 1:1000, Tonbo Biosciences), and fixed in 1% PFA/PBS. The next day, fixed cells were treated with anti-CD16/CD32 (1:100, Tonbo Biosciences) and then stained with antibodies that recognize surface lineage markers and analyzed by flow cytometry.

Livers were perfused by PBS injection into the inferior vena cava and out of the portal vein. Blanched livers were minced with sterile scissors and mashed against a 70 μM cell strainer. Hepatocytes and large debris were pelleted at 60 x *g* for 1 minute, 22°C, with no brake. Intrahepatic immune cell (IHIC) and residual hepatocyte containing supernatants were pelleted at 480 x *g* for 8 minutes, 22°C, with max brake and resuspended in 37.5% Percoll (Sigma-Aldrich)/cRPMI2. Remaining hepatocytes were separated from IHIC by centrifugation at 850 x *g* for 30 minutes, 22°C, with no brake. Red blood cells were removed from the resulting pellet with RBC lysis buffer (Tonbo Biosciences). Viable cells were quantified using trypan blue exclusion. IHIC and splenocytes (4×10^5) from infected or mock-infected mice were stained with a fluorescent viability dye (Ghost Dye Violet 450, 1:1000, Tonbo Biosciences), treated with anti-CD16/CD32 (1:100, Tonbo Biosciences), stained with antibodies that recognize surface lineage markers, and then fixed in 1% PFA/PBS. Fixed volumes of cell suspensions were analyzed by flow cytometry the next day. Absolute cell counts were determined by multiplying final number of lineage marker-positive cells by dilution factor used to normalize cell counts for antibody staining.

All primary cell samples were resuspended in 3% FBS/PBS and analyzed using a S1000 Flow Cytometer with a A600 96-well plate high throughput extension and compensated using CellCapture software (Stratedigm). Data was analyzed with FlowJo Software (Treestar). The flow gating strategy for liver and spleen immune cells is included in Extended Data Figure 9.

Statistical analysis

Differences in data were tested for significance using GraphPad Prism v8.3.1 for Windows (GraphPad). For details regarding the statistical tests applied, please refer to the figure

Author Manuscript Author Manuscript Author Manuscript Author Manuscript

legends. *P* values < 0.05 were considered significant. *P* values > 0.05 are listed by figure in Supplementary Table 4.

Data availability

The authors declare that the data supporting the findings of this study are available within the article and its Supplementary Information files or are available on request. The RNA-seq data discussed in this publication have been deposited in the Gene Expression Omnibus (GEO) database, https://www.ncbi.nlm.nih.gov/geo (GSE146074). Data used for scRNA-seq analysis of hAEC has been previously reported[38]. Data used for RNA-seq analysis of *LY6E* induction in hAEC after viral infection has been previously reported[39]. Genbank (https://www.ncbi.nlm.nih.gov/genbank/) accession numbers for viral gene sequences used to generate S protein pseudoparticles: VSV-G, NC_001560; HCoV-229E S, X16816; MERS-CoV S, JX869059; SARS-CoV S, AY291315.1, SARS-CoV-2, NCBI Reference Sequence: YP_009724390.1. NCBI accession number for generating expression plasmid for *C. dromedarius* LY6E, XM_031439745.1.

Author Manuscript
Author Manuscript
Author Manuscript
Author Manuscript

Extended Data

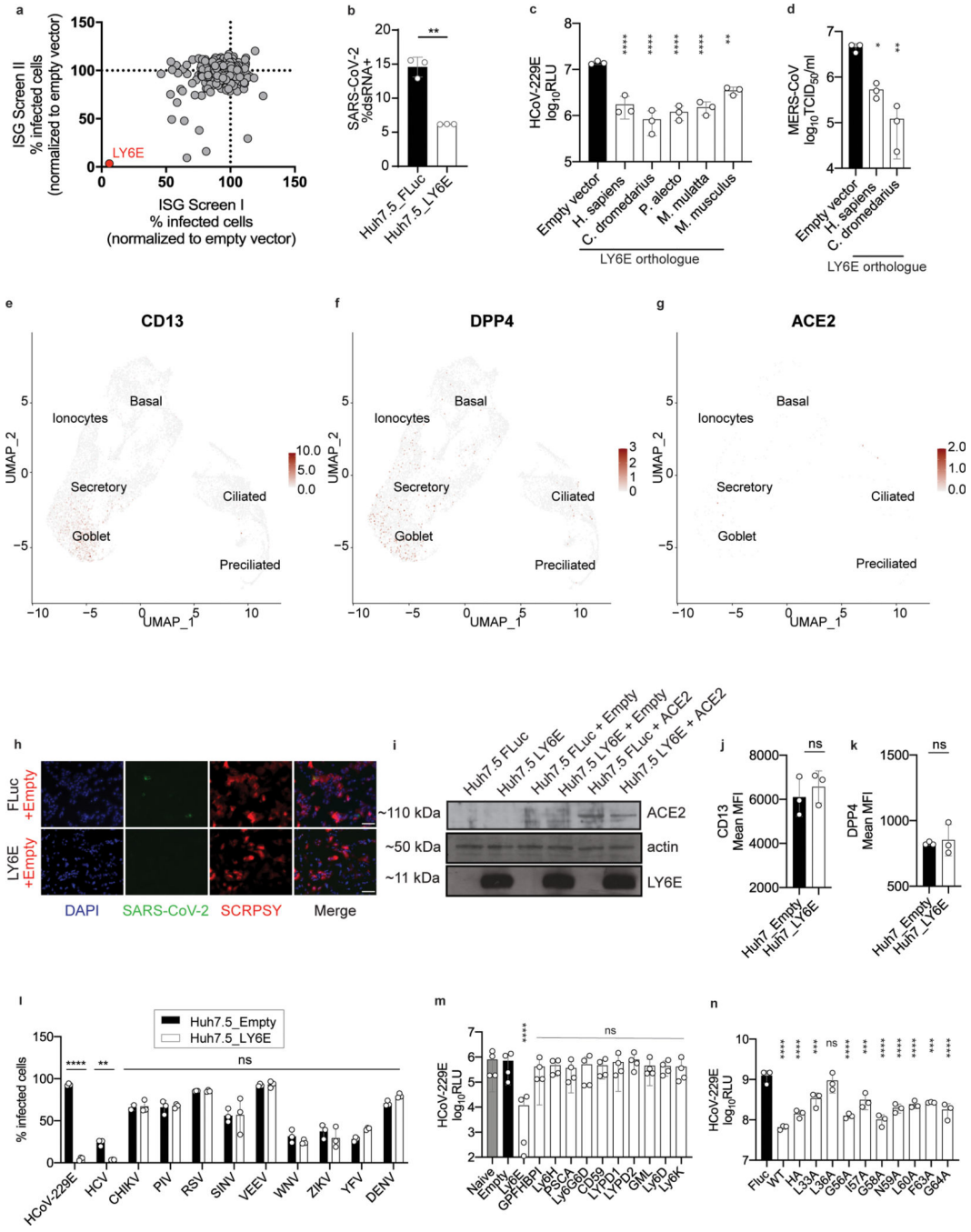

Extended Data Fig. 1. The antiviral activity of LY6E is conserved, independent of CoV receptors, and extends to HCV.

a, Duplicate screens depicting HCoV-229E infection (48 hours post-infection) in Huh7 cells expressing ISGs. **b**, SARS-CoV-2 infection of Huh7.5 cells expressing LY6E or a control (FLuc). **c**, HCoV-229E infection of Huh7.5 cells expressing vector control or human (*H. sapiens*), camel (*C. dromedarius*), bat (*P. alecto*), mouse (*M. musculus*), or rhesus (*M. mulatta*) LY6E orthologues. **d**, Stable LY6E or empty vector expressing Huh7.5 cells

Author Manuscript Author Manuscript Author Manuscript Author Manuscript

infected with MERS-CoV. **e-g**, UMAP visualization of *CD13* (**e**) *DPP4* (**f**), and *ACE2* (**g**) expression and distribution among distinct cell types in hAEC cultures from 2 donors by scRNA-seq. **h**, SARS-CoV-2 infection of LY6E or control vector (FLuc) Huh7.5 cells co-expressing control vector (empty). Blue: DAPI, green: SARS-CoV-2 dsRNA, red: TagRFP encoded in SCRPSY-ACE2 vector. **i**, Western blot of Huh7.5 expressing LY6E or FLuc and empty vector or ACE2. **j-k**, Stable LY6E or empty vector expressing Huh7 cells were assessed for cell surface expression of CD13 (**j**) and DPP4 (**k**). **l**, Stable Huh7.5 cells expressing either LY6E or empty vector infected with HCoV-229E, HCV, CHIKV, hPIV-3, RSV, SINV, VEEV, WNV, ZIKV, YFV, and DENV. **m**, HCoV-229E-Rluc infection of naïve or stably transduced Huh7 cells expressing empty vector control or LY6/uPAR family members. **n**, HCoV-229E-Rluc infection of Huh7 cells expressing control vector (FLuc), LY6E WT, LY6E HA or specific block mutants[9]. In **h**, scale bars are 100 μM. Immunofluorescence and western blot images are depicted exemplarily from n=3 (**h**) and n=3 (**i**). Data depicts mean of independent biological replicates, n=3 (**b-d,j-n**). Statistical significance was determined by two-tailed unpaired student's t-test with Welch's correction (**b**,**j-k**), ordinary one-way ANOVA with Dunnett`s correction for multiple comparison (**c-d, m-n**), two-way ANOVA followed by Sidak's multiple comparisons test (**l**). Error bars: SD (**b-d,j-n**). *P* values (left-to-right): **b**, ** p=0.0098; **c**, **** p=<0.0001, ** p=0.0030; **d**, * p=0.0118, ** p=0.0013; **l**, **** p=>0.0001, ** p=0.0095; **m**, **** p=<0.0001; **n**, **** p=<0.0001, <0.0001, *** p=0.0005, **** p=<0.0001, *** p=0.0003, **** p=<0.0001, <0.0001, <0.0001, *** p=0.0001, **** p=<0.0001.

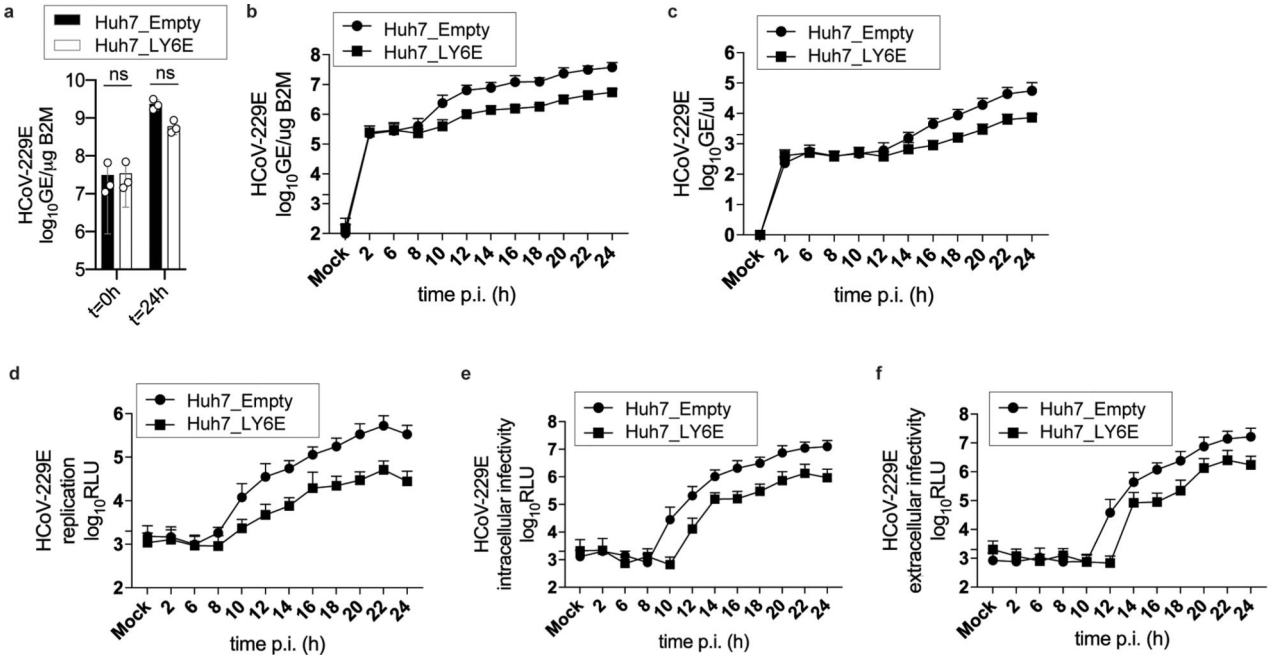

Extended Data Fig. 2. LY6E does not affect CoV binding, replication, translation, assembly, or release.

a, Stable LY6E expressing or empty control Huh7 cells were incubated with HCoV-229E and binding analyzed immediately (t=0 h) or after incubation for 24 hours (t=24 h) by RT-qPCR. **b-f**, Stable LY6E expressing or control Huh7 cells were mock-infected or infected

Author Manuscript Author Manuscript Author Manuscript Author Manuscript

with HCoV-229E-Rluc. Cell lysates were harvested at the indicated time points and intracellular viral RNA was extracted, and viral replication detected via qRT-PCR (**b**). Cell supernatant was harvested, extracellular viral RNA was extracted, and viral replication detected via qRT-PCR (**c**). Cell lysates were harvested, and intracellular Renilla luciferase activity was detected upon cell lysis (**d**). Cells were subjected to 3 rounds of freeze/thaw cycles. Cell debris was removed, and the supernatant titrated on naïve Huh7 cells. Intracellular infectivity was determined (**e**). Supernatant was harvested and titrated on naïve Huh7 cells to determine extracellular infectivity (**f**). Data represent mean of independent biological replicates, n=3 (**a-f**). Statistical significance was determined by two-way ANOVA followed by Sidak's multiple comparisons test (**a**). Error bars: SD (**a-f**).

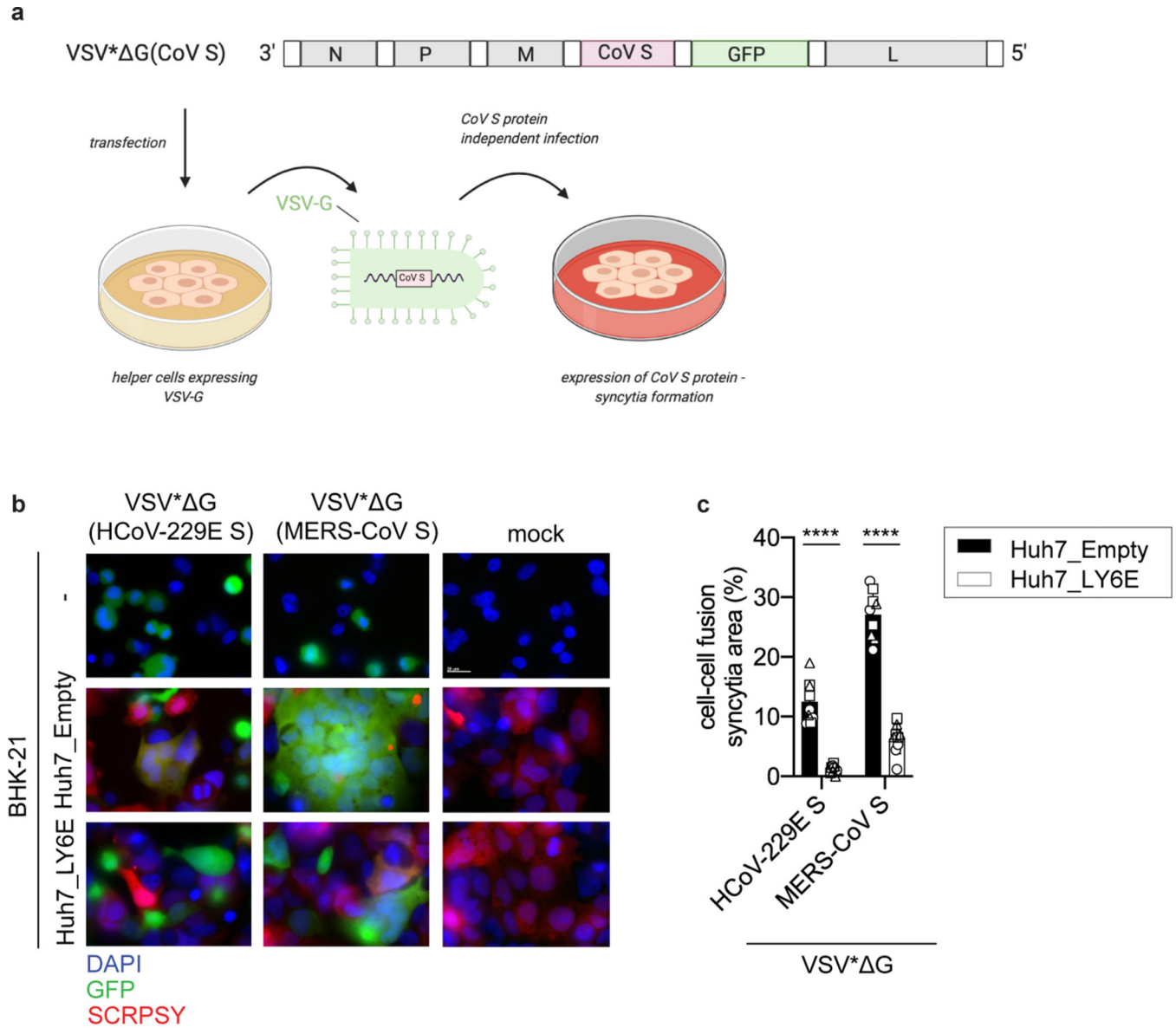

Extended Data Fig. 3. Generation of recombinant VSV vector driving CoV S protein expression (VSV*ΔG(CoV)) and heterologous cell-cell fusion assay.

Author Manuscript Author Manuscript Author Manuscript Author Manuscript

a, Schematic depiction of the generation of recombinant VSV*ΔG(CoV S) expressing both CoV S protein and GFP reporter protein. The respective CoV S genes were inserted into the genomic VSV*ΔG cDNA and recombinant virus was generated in BHK-G43 cells expressing the VSV G protein. The recombinant virus produced in this way harbored the VSV G protein in the envelope allowing CoV S protein-independent infection of cells. Infection of cells with VSV*ΔG(CoV S) led to the expression of CoV S protein and consequent syncytia formation. **b**, Heterologous syncytia formation assay. BHK-21 cells were infected with VSV G protein trans-complemented VSV*ΔG(CoV S) viruses or were mock-infected, followed by co-culture with LY6E or empty control Huh7 cells. Syncytia formation was determined. Blue: DAPI, green: GFP, red: TagRFP encoded in SCRPSY vector. **c**, Quantification of VSV*ΔG(CoV S) induced syncytia depicted as percentage syncytia area. Three independent areas were analyzed per biological replicate (circle, square, triangle). Data represent mean of independent biological replicates, n=3 (**c**). In **b**, scale bar is 20 μM. Statistical significance was determined by two-way ANOVA followed by Sidak's multiple comparisons test (**c**). Error bars: SD. *P* values: **c** (left-to-right), **** $p=6.0 \times 10^{-9}$, **** $p=1.1 \times 10^{-15}$.

Author Manuscript
Author Manuscript
Author Manuscript
Author Manuscript

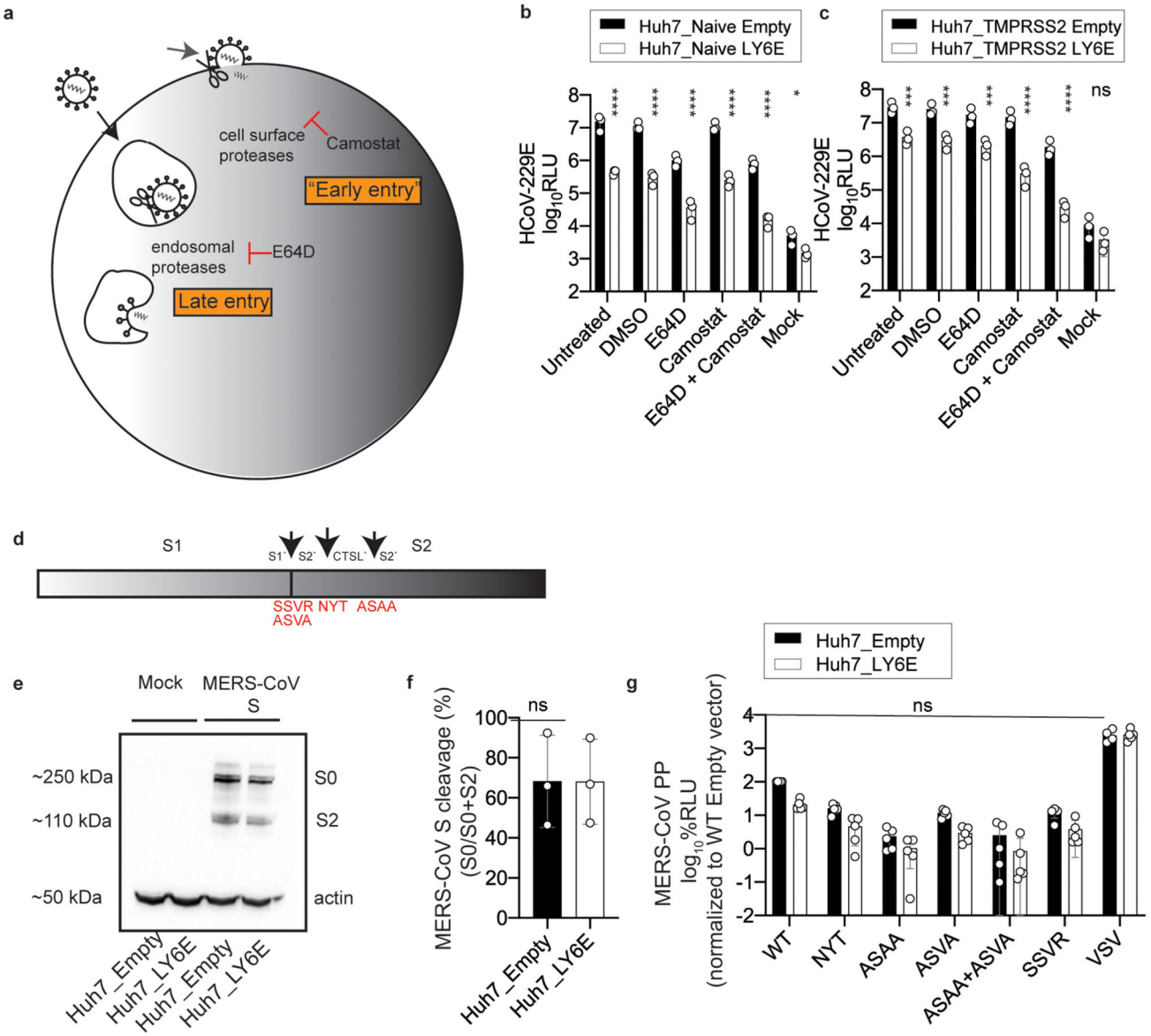

Extended Data Fig. 4. The antiviral effect of LY6E is independent of proteolytic cleavage of CoV spike protein.

a, Schematic depiction of cell entry routes of CoVs and intervention by selected compounds. **b-c**, LY6E or empty control-expressing Huh7 cells naïve for (**b**) or ectopically overexpressing TMPRSS2 (**c**) were pre-treated with the indicated compounds before infection with HCoV-229E-Rluc. **d**, Schematic depiction of the CoV spike (S) protein containing the subunits S1 and S2. Arrows indicate the S1/S2' cleavage site, a proposed cleavage site for cathepsin L (CTSL') and the S2' cleavage site. Amino acid exchanges disrupting the respective cleavage sites are depicted in red. **e**, Western blot of S cleavage in LY6E or empty control-expressing Huh7 cells transfected with a plasmid encoding for MERS-CoV S protein (S0= uncleaved, S2= S2 subunit). **f**, MERS CoV S cleavage was analyzed by quantification of S0 and S2 bands. **g**, LY6E or empty control-expressing Huh7 cells inoculated with CoV-pseudoparticles (pp) harboring MERS-CoV S WT or MERS-CoV

S proteins containing various cleavage site mutations. Data represent mean of independent biological replicates, n=3 (**b**), n=3 (**c**), n=3 (**e**), n=3 (**f**), n=5 (**g**). Statistical significance was determined by two-way ANOVA followed by Sidak's multiple comparisons (**b-c, g**) or two-tailed unpaired student's t-test with Welch's correction (**f**). Error bars: SD. *P* values (left-to-right): **b**, **** p=4.4 × 10^{-9}, p=1.6 × 10^{-9}, p=6.2 × 10^{-9}, p=7.5 × 10^{-10}, p=3.0 × 10^{-10}, * p=0.0179; **c**, *** p=0.0007, p=0.0005, p=0.0006, **** p=4.8 × 10^{-8}, p=1.8 × 10^{-8}.

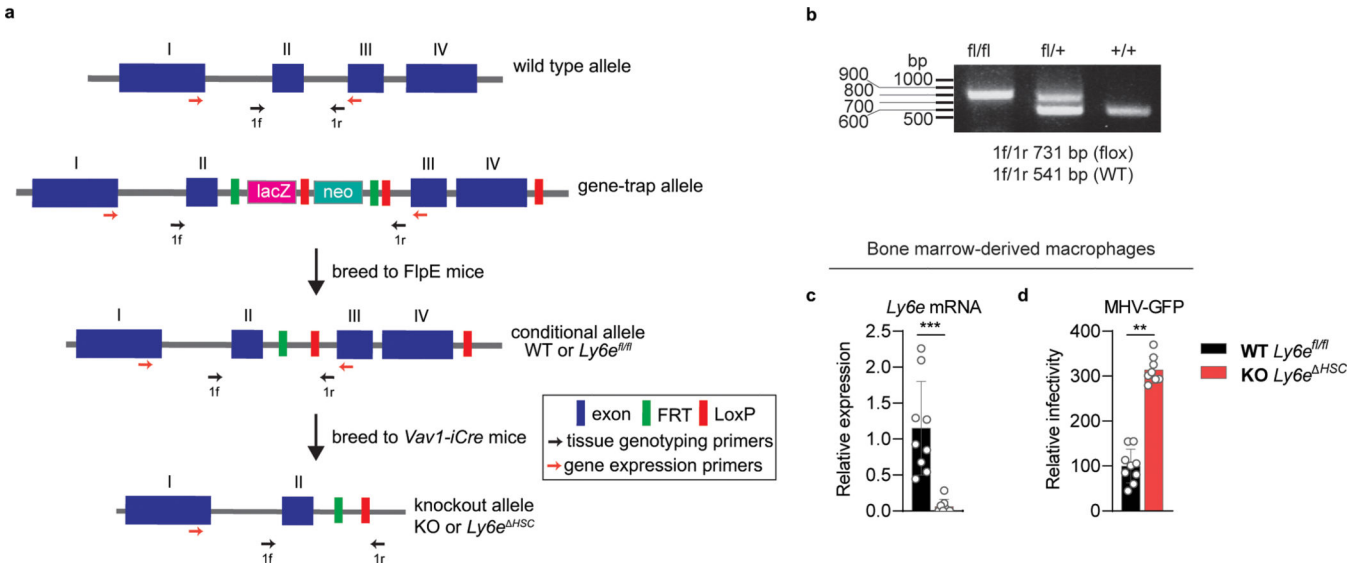

Extended Data Fig. 5. Generation of hematopoietic Ly6e conditional knockout mouse.

a, Strategy used to generate *Ly6e*$^{\Delta HSC}$ mice. Hematopoietic-tissue specific ablation of Ly6e was achieved by crossing *Ly6e*$^{fl/fl}$ mice with transgenic *Vav1-iCre* mice to remove the LoxP-flanked exon III and IV, resulting in a 17 amino acid truncated variant of the 130 amino acid full-length protein. Primers used for tissue genotyping and gene expression are also depicted as arrows. **b,** Gel electrophoresis of tissue genotyping PCR, representing *Ly6e*$^{fl/fl}$, *Ly6e*$^{fl/+}$, and *Ly6e*$^{+/+}$ mice. **c**, *Ly6e* gene expression in bone marrow-derived macrophages (BMDM). **d,** Infection of BMDM. For **c-d**, n=9 (*Ly6e*$^{fl/fl}$) or n=8 (*Ly6e*$^{\Delta HSC}$) mice from three pooled experiments. The gel shown in **b** is representative of all genotyping performed to identify *Ly6e*$^{fl/fl}$ mice. Data for **c-d** is shown normalized to *Ly6e*$^{fl/fl}$ values. Statistical significance was determined by using two-tailed unpaired student's t-test with Welch's correction (**c**) or two-tailed ratio-paired t-test (**d**). Data are presented as mean values ± SD (**c-d**). *P* values: **c**, *** p=0.0010. **d**, ** p=0.0021.

Author Manuscript Author Manuscript Author Manuscript Author Manuscript

Author Manuscript Author Manuscript Author Manuscript Author Manuscript

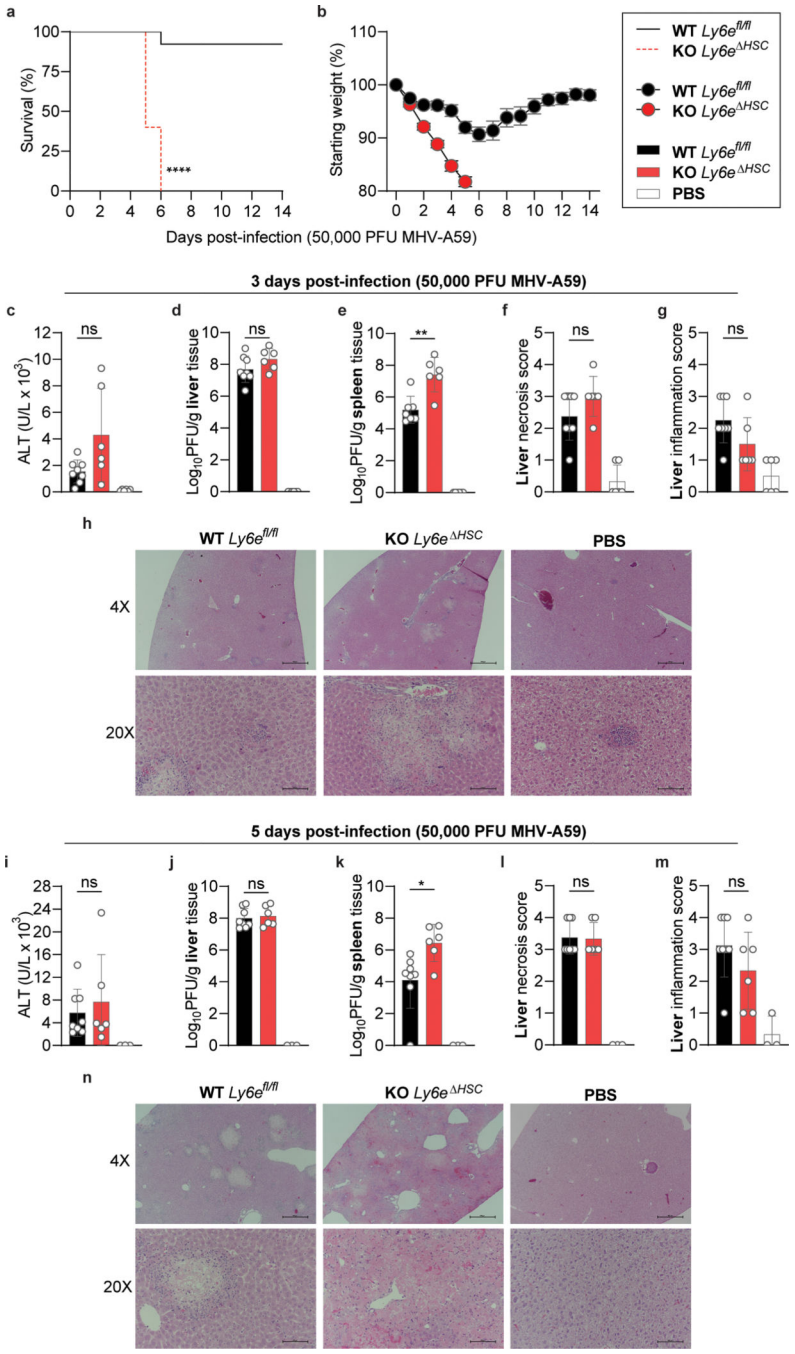

Extended Data Fig. 6. *Ly6e*$^{\Delta HSC}$ mice are susceptible to mouse hepatitis virus.

a-b, Male *Ly6e*$^{fl/fl}$ and *Ly6e*$^{\Delta HSC}$ mice injected with PBS or MHV and monitored for survival (**a**) and weight loss (**b**). **c-n,** Mice were euthanized at 3- (**c-h**) or 5- **(i-n**) days post-infection for determination of serum ALT (**c,i**), viral titers in liver (**d,j**) and spleen (**e,k**), and liver necrosis and inflammation (**f-h**, **l-n**). For **a-b**, n=15 for days 0–6, n=14 for days 6–14, (*Ly6e*$^{fl/fl}$), n=10 for days 0–5, n=4 for days 5–6, n=0 for days 6–14 (*Ly6e*$^{\Delta HSC}$) from three pooled experiments. For **c-g**, n=8 (*Ly6e*$^{fl/fl}$,), n=6 (*Ly6e*$^{\Delta HSC}$), or n=6 (PBS) from two pooled experiments; images shown in **h** are representative of the same cohorts. For **i-m**, n=8

(*Ly6e*$^{fl/fl}$,), n=6 (*Ly6e*$^{\Delta HSC}$), or n=3 (PBS) from two pooled experiments; images shown in **n** are representative of the same cohorts. In **h,n**, scale bars are 500 μM (4x) and 100 μM (20x). Significance for was tested by two-sided Mantel-Cox test (**a**), two-tailed unpaired student's t-test with Welch's correction (**c-e**, **i-k**), two-tailed Mann-Whitney U test (**f-g**, **l-m**). Data are presented as mean values ± SEM (**b**) or SD (**c-g**, **i-m**). *P* value: **a**, **** p=3.946 × 10^{-6}; **e**, ** p=0.0026; **k**, * p=0.0119.

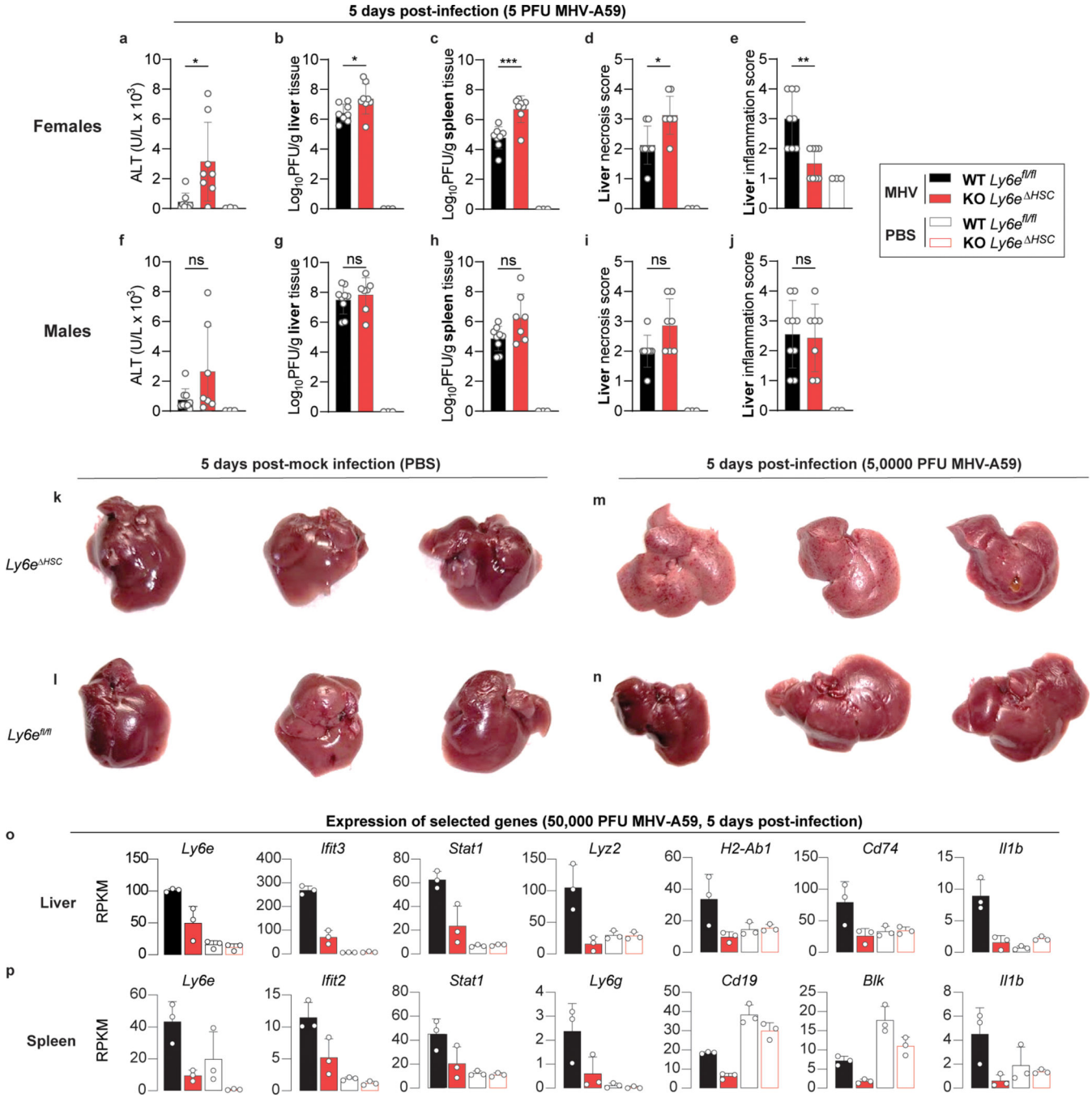

Extended Data Fig. 7. *Ly6e*$^{\Delta HSC}$ mice have enhanced sensitivity to mouse hepatitis virus and a differential gene expression profile.

Author Manuscript Author Manuscript Author Manuscript Author Manuscript

Author Manuscript Author Manuscript Author Manuscript Author Manuscript

a-j, Female (**a-e**) and male (**f-g**) *Ly6e*$^{fl/fl}$ and *Ly6e*$^{\Delta HSC}$ mice injected with PBS or MHV and assessed for serum ALT (**a**,**f**), viral titers in liver (**b**,**g**) and spleen (**c**,**h**), and liver necrosis and inflammation (**d-e**, **i-j**). **k-n**, Female *Ly6e*$^{fl/fl}$ and *Ly6e*$^{\Delta HSC}$ mice injected with PBS or MHV and whole livers were imaged. Mock-infected (PBS) *Ly6e*$^{\Delta HSC}$ mice (**k**), mock-infected *Ly6e*$^{fl/fl}$ mice (**l**), MHV-infected *Ly6e*$^{\Delta HSC}$ mice (**m**), MHV-infected *Ly6e*$^{fl/fl}$ mice (**n**). **o-p**, Representative genes from transcriptomic analysis of liver (**o**) and spleen (**p**) from MHV-infected and PBS-injected female *Ly6e*$^{fl/fl}$ and *Ly6e*$^{\Delta HSC}$ mice. For **a-e**, n=8 (*Ly6e*$^{fl/fl}$,), n=8 (*Ly6e*$^{\Delta HSC}$), or n=3 (PBS) from two pooled experiments per sex. For **f-j**, n=9 (*Ly6e*$^{fl/fl}$,), n=7 (*Ly6e*$^{\Delta HSC}$), or n=3 (PBS) two pooled experiments. For **k-p**, n=3. Statistical significance was determined by two-tailed unpaired student's t-test with Welch's correction (**a-c**, **f-h**), two-tailed Mann-Whitney U test (**d-e**, **i-j**). Data are presented as mean values ± SD (**a-j**; **o-p**). *P* value: **a**, * p=0.0234; **b**, * p=0.0428; **c**, *** p=0.0004; **d,** * p=0.0210; **e**, ** p=0.0054.

Author Manuscript Author Manuscript Author Manuscript Author Manuscript

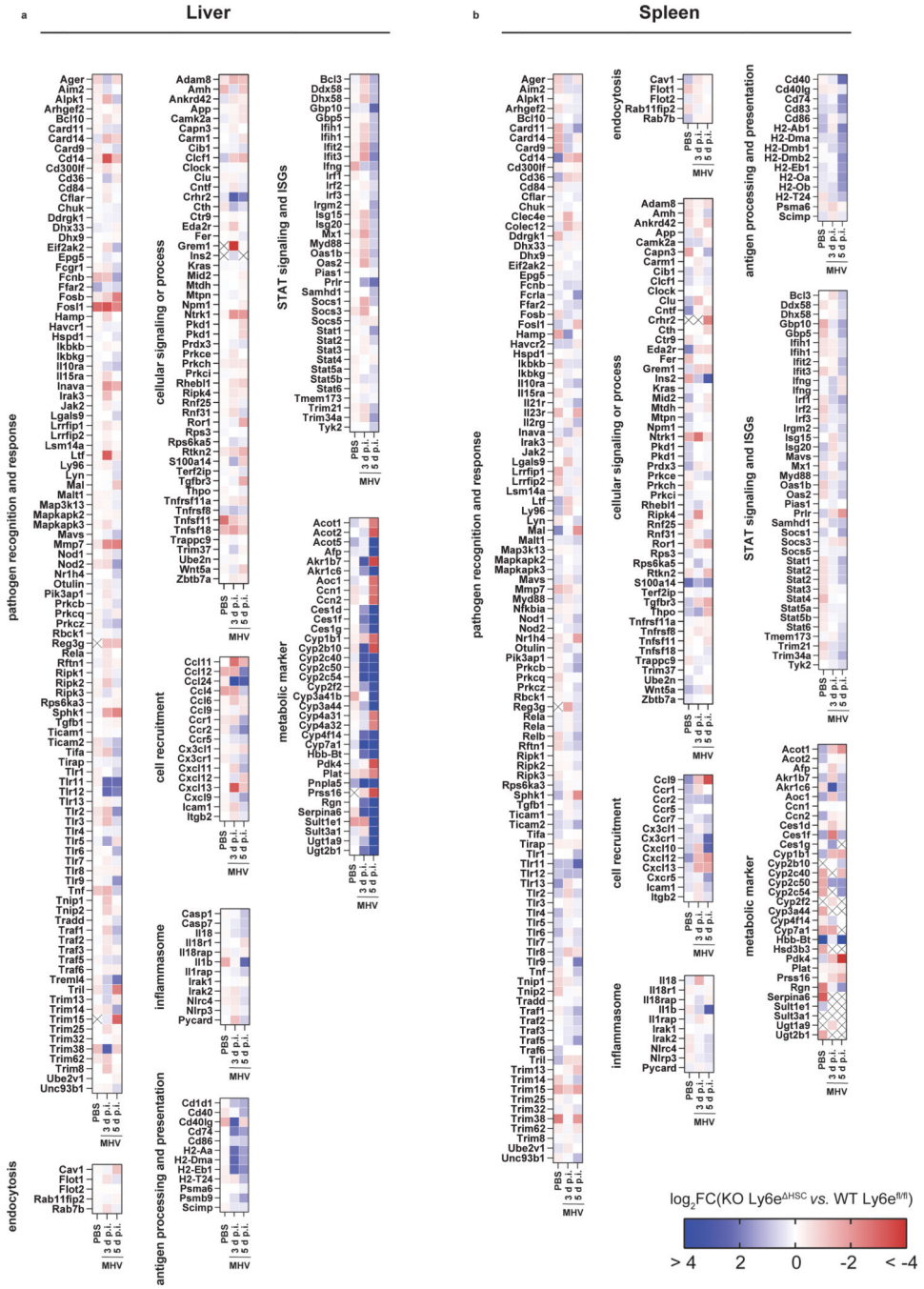

Extended Data Fig. 8. Dynamic transcriptional changes in liver and spleen of *Ly6e*$^{\Delta HSC}$ vs *Ly6e*$^{fl/fl}$ mice.

Depicted are fold changes in liver and spleen gene expression from *Ly6e*$^{\Delta HSC}$ mice compared to *Ly6e*$^{fl/fl}$ mice. RPKM values from RNA-seq data for liver (**a**) and spleen (**b**) were used to calculate fold changes. Crossed out genes were not detected in either KO or WT mice at respective conditions.

Author Manuscript Author Manuscript Author Manuscript Author Manuscript

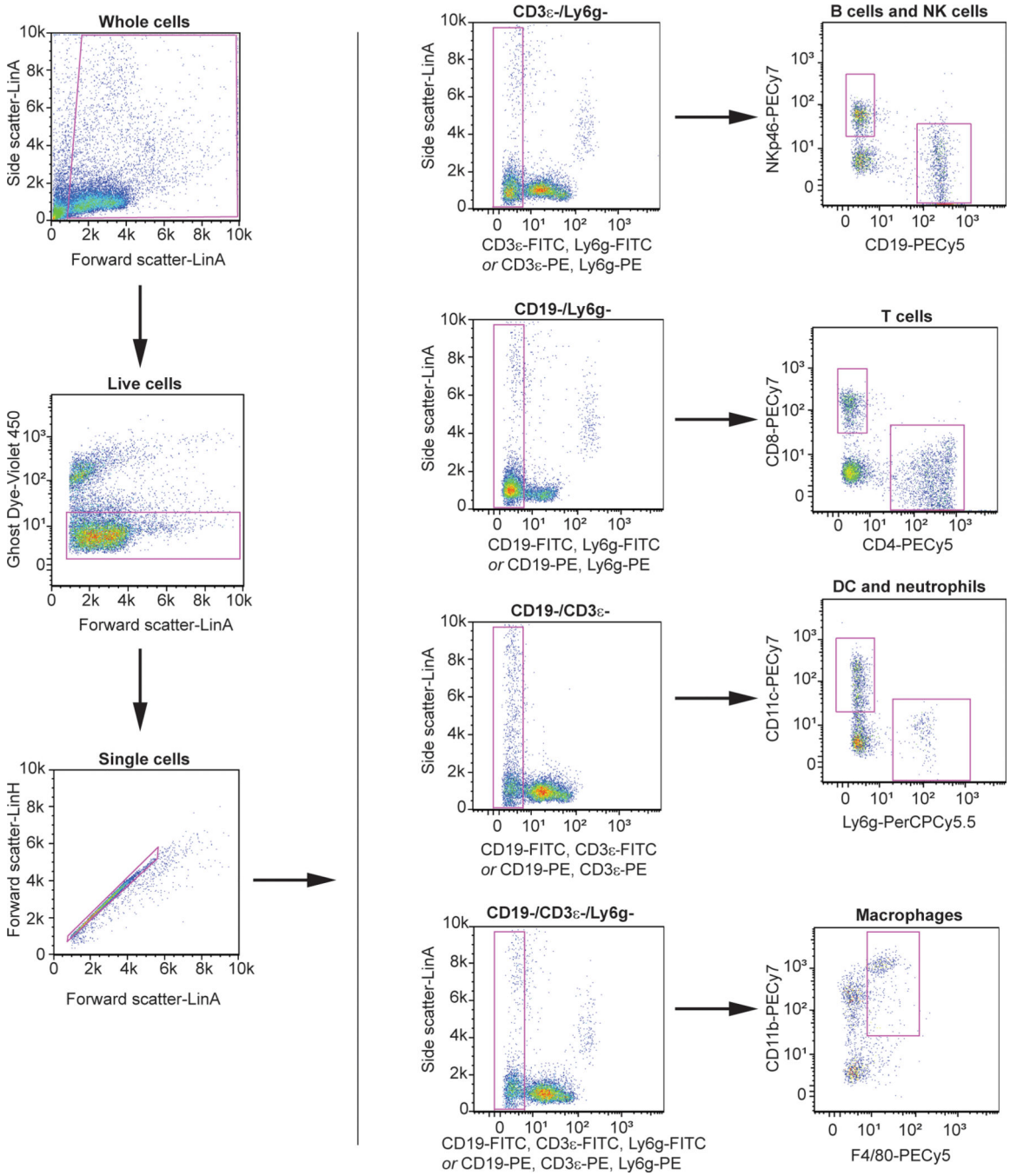

Extended Data Fig. 9. Gating strategy for intrahepatic and splenic immune cell identification.

Antibody-stained suspensions of isolated intrahepatic immune cells or splenic immune cells were first analyzed by forward scatter/side scatter to remove debris events, then gated for exclusion of a viability dye (Ghost Dye Violet 450), and finally for selection of single cell events. A dump-gate strategy was used to identify immune cell populations as indicated in the diagram. FITC-conjugated fluorophores were used for immunophenotyping experiments and PE-conjugated fluorophores were used for *ex vivo* infections.

Author Manuscript
Author Manuscript
Author Manuscript
Author Manuscript

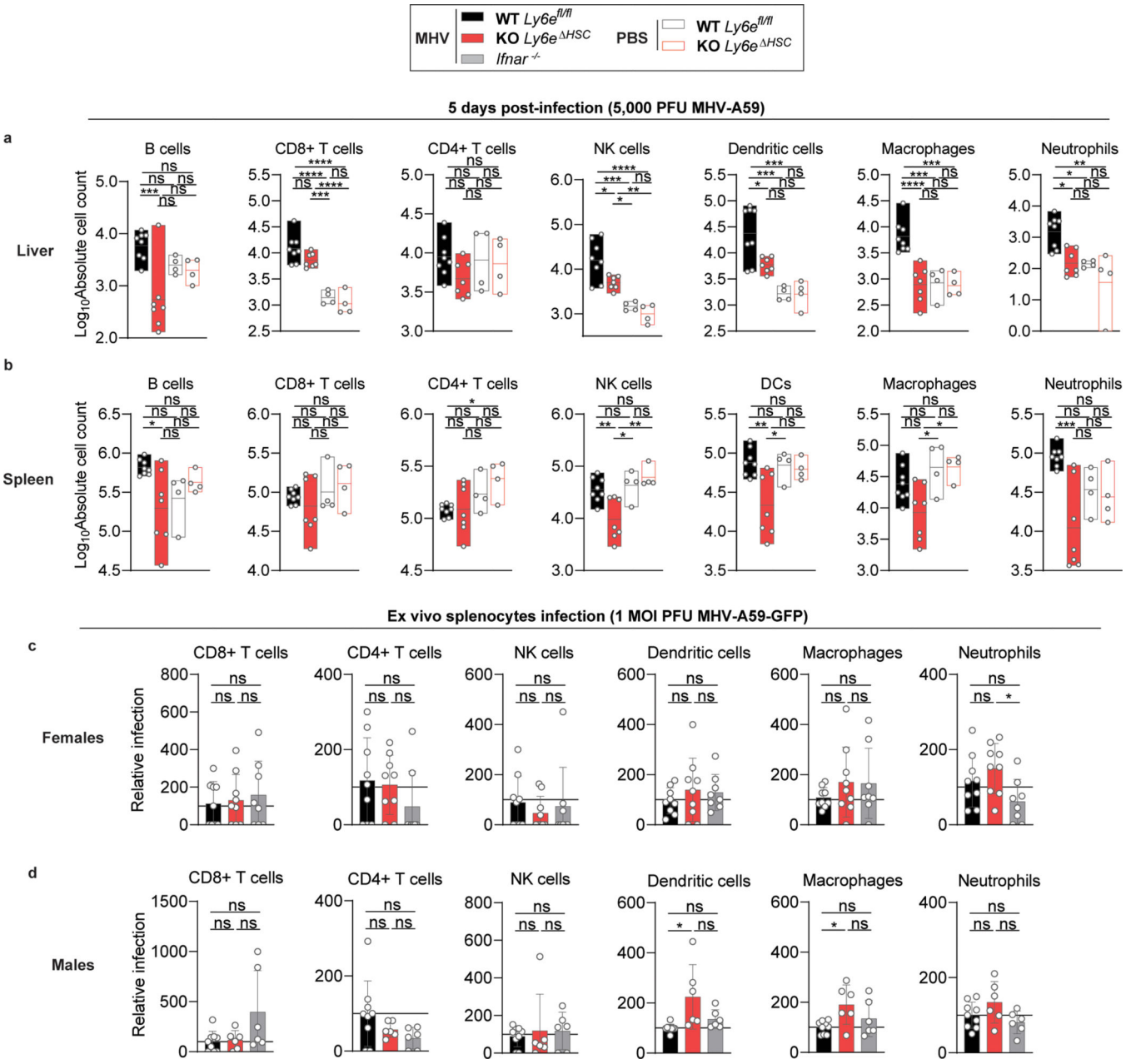

Extended Data Fig. 10. *Ly6e* protects immune cells from mouse hepatitis virus infection.

a-b, Immune cell counts from liver (**a**) and spleen (**b**) of MHV-infected or PBS-injected male mice. **c-d**, Infection of cultured splenocytes from females (**c**) and males (**d**) normalized to average (line at 100) of *Ly6e*$^{fl/fl}$ mice. For **a-b**, n=8 (infected *Ly6e*$^{fl/fl}$), n=7 (infected *Ly6e*$^{\Delta HSC}$), n=4 PBS-injected from two pooled experiments. For **c**, n=9 (*Ly6e*$^{fl/fl}$ and *Ly6e*$^{\Delta HSC}$) and n=8 (*Ifnar*−/−) from four pooled experiments. For **d**, n=9 (*Ly6e*$^{fl/fl}$), n=6 (*Ly6e*$^{\Delta HSC}$), or n=6 (*Ifnar*$^{-/-}$) mice from four pooled experiments. Statistical significance was determined by one-way ANOVA with Tukey's multiple comparisons test (**a-d**). For box plots, center line indicates mean and upper and lower bounds respectively indicate maximum and minimum replicate values (**a-b**). Data are presented as mean values ± SD (**a-d**). *P* values

Author Manuscript Author Manuscript Author Manuscript Author Manuscript

(top-bottom, then left-right): **a**, *** p=0.0008; **** p=5.6844 × 10^{-7}, **** p=3.1123 × 10^{-6}, **** p=2.337 × 10^{-5}, *** p=0.0002; **** p=1.7135 × 10^{-5}, *** p=0.0001, * p=0.0216, ** p =0.0075, * p=0.0494; *** p=0.0002, *** p=0.0002, ns p=0.9999, * p=0.0182; *** p=0.0004, *** p=0.0008, **** p=7.354 × 10^{-5}; ** p=0.0011, * p=0.0421, * p=0.0160, **b**, * p=0.0215; * p=0.0449; ** p=0.0081, ** p=0.0022, * p=0.0131; ** p=0.0044, * p=0.0299; * p=0.0179, * p=0.0194; *** p=0.0007. **c**, * p=0.0288; **d**, * p=0.0104; * p=0.0240.

Supplementary Material

Refer to Web version on PubMed Central for supplementary material.

Acknowledgements

We would like to thank the following people for their generous contribution of reagents and infrastructure which greatly enhanced this study, especially the sequencing facility in Bern, the diagnostic facility of IVI, and the Animal Resource Center at UTSW. Furthermore, we are grateful to Robin Pohorelsky, Shay Elias, and Nina Garcia from the UTSW Animal Resource Center for assisting in the *in vivo* experiments. We are grateful to Samira Locher (IVI, Bern, Switzerland) for cloning the MERS spike cDNA. Furthermore, we would like to thank Berend Jan Bosch, Marcel Müller and Christian Drosten for reagents and the SARS-CoV-2 virus stocks. We thank the following investigators for contributing viral molecular clones or viral stocks: P.L. Collins (RSV, hPIV-3), I. Frolov (VEEV), M.T. Heise (SINV), S. Higgs (CHIKV), and the CDC (ZIKV).

Finally, we'd like to thank all members, past and present, of Institute of Virology and Immunology, the Schoggins lab, and the Rice lab for useful discussions.

S.P. was supported by the European Commission's Horizon 2020 Research and Innovation Program under the Marie Skłodowska-Curie grant agreement 748627 and the Swiss National Science Foundation (SNF; grant 310030 173085). K.B.M. and J.W.S. were supported in part by The Clayton Foundation and The American Lung Association. J.W.S. was additionally supported by NIH grant AI117922 and a Burroughs Wellcome Fund 'Investigators in the Pathogenesis of Infectious Diseases' Award. K.B.M. was additionally supported by NIH Training Grant AI005284. S.Pö. was supported by BMBF, RAPID Consortium, grant 01KI1723D. N.H. was supported by NIH grant AI132751. E.M., H.H.H., M.S. and C.M.R. were supported in part by NIH grants AI091707, AI091707–10S1, and The G. Harold and Leila Y. Mathers Charitable Foundation. R.D. was supported by the Swiss National Science Foundation (SNF; grant:179260). G.Z. was supported by a grant from the Swiss National Science Foundation grant 166265. P.V. and J.K. were supported by the Swiss National Science Foundation (SNF; grants: 310030_173085 (P.V. and J.K.) and CRSII3_160780 (J.K.)). A.K. was supported by the Federal Ministry of Education and Research (BMBF; grant RAPID, #01KI1723A). V.T. was supported by the Swiss National Science Foundation (SNF; grants: 310030_173085; CRSII3_160780), and the Federal Ministry of Education and Research (BMBF; grant RAPID, #01KI1723A). I.N.B. and M.B.M were supported by the National Science Foundation Graduate Research Fellowship under Grants No. 2016217834 and 2019274212, respectively.

References

1. Zhu N. et al. A Novel Coronavirus from Patients with Pneumonia in China, 2019. N Engl J Med, doi:10.1056/NEJMoa2001017 (2020).
2. Drosten C. et al. Identification of a novel coronavirus in patients with severe acute respiratory syndrome. N Engl J Med 348, 1967–1976, doi:10.1056/NEJMoa030747 (2003). [PubMed: 12690091]
3. Zaki AM, van Boheemen S, Bestebroer TM, Osterhaus AD & Fouchier RA Isolation of a novel coronavirus from a man with pneumonia in Saudi Arabia. N Engl J Med 367, 1814–1820, doi:10.1056/NEJMoa1211721 (2012). [PubMed: 23075143]
4. Kindler E, Thiel V & Weber F Interaction of SARS and MERS Coronaviruses with the Antiviral Interferon Response. Adv Virus Res 96, 219–243, doi:10.1016/bs.aivir.2016.08.006 (2016). [PubMed: 27712625]

Author Manuscript Author Manuscript Author Manuscript Author Manuscript

5. Corman VM, Muth D, Niemeyer D & Drosten C Hosts and Sources of Endemic Human Coronaviruses. Adv Virus Res 100, 163–188, doi:10.1016/bs.aivir.2018.01.001 (2018). [PubMed: 29551135]
6. Wang BX & Fish EN Global virus outbreaks: Interferons as 1st responders. Semin Immunol 43, 101300, doi:10.1016/j.smim.2019.101300 (2019).
7. Cervantes-Barragan L. et al. Control of coronavirus infection through plasmacytoid dendritic-cell-derived type I interferon. Blood 109, 1131–1137, doi:10.1182/blood-2006-05-023770 (2007). [PubMed: 16985170]
8. Schoggins JW Interferon-Stimulated Genes: What Do They All Do? Annu Rev Virol 6, 567–584, doi:10.1146/annurev-virology-092818-015756 (2019). [PubMed: 31283436]
9. Schoggins JW et al. A diverse range of gene products are effectors of the type I interferon antiviral response. Nature 472, 481–485, doi:10.1038/nature09907 (2011). [PubMed: 21478870]
10. Dittmann M. et al. A serpin shapes the extracellular environment to prevent influenza A virus maturation. Cell 160, 631–643, doi:10.1016/j.cell.2015.01.040 (2015). [PubMed: 25679759]
11. Mar KB et al. LY6E mediates an evolutionarily conserved enhancement of virus infection by targeting a late entry step. Nature Communications 9, 3603, doi:10.1038/s41467-018-06000-y (2018).
12. Hackett BA & Cherry S Flavivirus internalization is regulated by a size-dependent endocytic pathway. Proc Natl Acad Sci U S A 115, 4246–4251, doi:10.1073/pnas.1720032115 (2018). [PubMed: 29610346]
13. Yu J, Liang C & Liu SL Interferon-inducible LY6E Protein Promotes HIV-1 Infection. J Biol Chem 292, 4674–4685, doi:10.1074/jbc.M116.755819 (2017). [PubMed: 28130445]
14. Yu J, Liang C & Liu SL CD4-Dependent Modulation of HIV-1 Entry by LY6E. J Virol 93, doi:10.1128/JVI.01866-18 (2019).
15. Upadhyay G Emerging Role of Lymphocyte Antigen-6 Family of Genes in Cancer and Immune Cells. Front Immunol 10, 819, doi:10.3389/fimmu.2019.00819 (2019). [PubMed: 31068932]
16. Hoffmann M, Kleine-Weber H & Pohlmann S A Multibasic Cleavage Site in the Spike Protein of SARS-CoV-2 Is Essential for Infection of Human Lung Cells. Mol Cell, doi:10.1016/j.molcel.2020.04.022 (2020).
17. Xia S. et al. Inhibition of SARS-CoV-2 (previously 2019-nCoV) infection by a highly potent pan-coronavirus fusion inhibitor targeting its spike protein that harbors a high capacity to mediate membrane fusion. Cell Res 30, 343–355, doi:10.1038/s41422-020-0305-x (2020). [PubMed: 32231345]
18. Heald-Sargent T & Gallagher T Ready, set, fuse! The coronavirus spike protein and acquisition of fusion competence. Viruses 4, 557–580, doi:10.3390/v4040557 (2012). [PubMed: 22590686]
19. Park JE et al. Proteolytic processing of Middle East respiratory syndrome coronavirus spikes expands virus tropism. Proc Natl Acad Sci U S A 113, 12262–12267, doi:10.1073/pnas.1608147113 (2016). [PubMed: 27791014]
20. Kleine-Weber H, Elzayat MT, Hoffmann M & Pohlmann S Functional analysis of potential cleavage sites in the MERS-coronavirus spike protein. Sci Rep 8, 16597, doi:10.1038/s41598-018-34859-w (2018). [PubMed: 30413791]
21. Langford MB, Outhwaite JE, Hughes M, Natale DRC & Simmons DG Deletion of the Syncytin A receptor Ly6e impairs syncytiotrophoblast fusion and placental morphogenesis causing embryonic lethality in mice. Sci Rep 8, 3961, doi:10.1038/s41598-018-22040-2 (2018). [PubMed: 29500366]
22. Matthews AE et al. Antibody is required for clearance of infectious murine hepatitis virus A59 from the central nervous system, but not the liver. J Immunol 167, 5254–5263, doi:10.4049/jimmunol.167.9.5254 (2001). [PubMed: 11673540]
23. Phares TW et al. CD4 T cells promote CD8 T cell immunity at the priming and effector site during viral encephalitis. J Virol 86, 2416–2427, doi:10.1128/JVI.06797-11 (2012). [PubMed: 22205741]
24. Wijburg OL, Heemskerk MH, Sanders A, Boog CJ & Van Rooijen N Role of virus-specific CD4+ cytotoxic T cells in recovery from mouse hepatitis virus infection. Immunology 87, 34–41 (1996). [PubMed: 8666433]

Author Manuscript Author Manuscript Author Manuscript Author Manuscript

25. Wijburg OL, Heemskerk MH, Boog CJ & Van Rooijen N Role of spleen macrophages in innate and acquired immune responses against mouse hepatitis virus strain A59. Immunology 92, 252–258, doi:10.1046/j.1365-2567.1997.00340.x (1997). [PubMed: 9415034]
26. Cervantes-Barragan L. et al. Type I IFN-mediated protection of macrophages and dendritic cells secures control of murine coronavirus infection. J Immunol 182, 1099–1106 (2009). [PubMed: 19124753]
27. Weiss SR & Leibowitz JL Coronavirus pathogenesis. Adv Virus Res 81, 85–164, doi:10.1016/B978-0-12-385885-6.00009-2 (2011). [PubMed: 22094080]
28. Eriksson KK, Cervantes-Barragan L, Ludewig B & Thiel V Mouse hepatitis virus liver pathology is dependent on ADP-ribose-1“-phosphatase, a viral function conserved in the alpha-like supergroup. J Virol 82, 12325–12334, doi:10.1128/JVI.02082-08 (2008). [PubMed: 18922871]
29. Karnam G. et al. CD200 receptor controls sex-specific TLR7 responses to viral infection. PLoS Pathog 8, e1002710, doi:10.1371/journal.ppat.1002710 (2012).
30. Lalezari JP et al. Enfuvirtide, an HIV-1 fusion inhibitor, for drug-resistant HIV infection in North and South America. N Engl J Med 348, 2175–2185, doi:10.1056/NEJMoa035026 (2003). [PubMed: 12637625]
31. Richardson RB et al. A CRISPR screen identifies IFI6 as an ER-resident interferon effector that blocks flavivirus replication. Nat Microbiol 3, 1214–1223, doi:10.1038/s41564-018-0244-1 (2018). [PubMed: 30224801]
32. Torriani G. et al. Identification of Clotrimazole Derivatives as Specific Inhibitors of Arenavirus Fusion. J Virol 93, doi:10.1128/JVI.01744-18 (2019).
33. Gierer S. et al. The spike protein of the emerging betacoronavirus EMC uses a novel coronavirus receptor for entry, can be activated by TMPRSS2, and is targeted by neutralizing antibodies. J Virol 87, 5502–5511, doi:10.1128/JVI.00128-13 (2013). [PubMed: 23468491]
34. Hoffmann M. et al. Differential sensitivity of bat cells to infection by enveloped RNA viruses: coronaviruses, paramyxoviruses, filoviruses, and influenza viruses. PLoS One 8, e72942, doi:10.1371/journal.pone.0072942 (2013).
35. Qing E, Hantak M, Perlman S & Gallagher T Distinct Roles for Sialoside and Protein Receptors in Coronavirus Infection. mBio 11, doi:10.1128/mBio.02764-19 (2020).
36. Skarnes WC et al. A conditional knockout resource for the genome-wide study of mouse gene function. Nature 474, 337–342, doi:10.1038/nature10163 (2011). [PubMed: 21677750]
37. Agac D, Estrada LD, Maples R, Hooper LV & Farrar JD The beta2-adrenergic receptor controls inflammation by driving rapid IL-10 secretion. Brain Behav Immun 74, 176–185, doi:10.1016/j.bbi.2018.09.004 (2018). [PubMed: 30195028]
38. Kelly JN et al. Comprehensive single cell analysis of pandemic influenza A virus infection in the human airways uncovers cell-type specific host transcriptional signatures relevant for disease progression and pathogenesis. bioRxiv (2020).
39. V’kovski P. et al. Disparate temperature-dependent virus – host dynamics for SARS-CoV-2 and SARS-CoV in the human respiratory epithelium. bioRxiv (2020).

Author Manuscript Author Manuscript Author Manuscript Author Manuscript

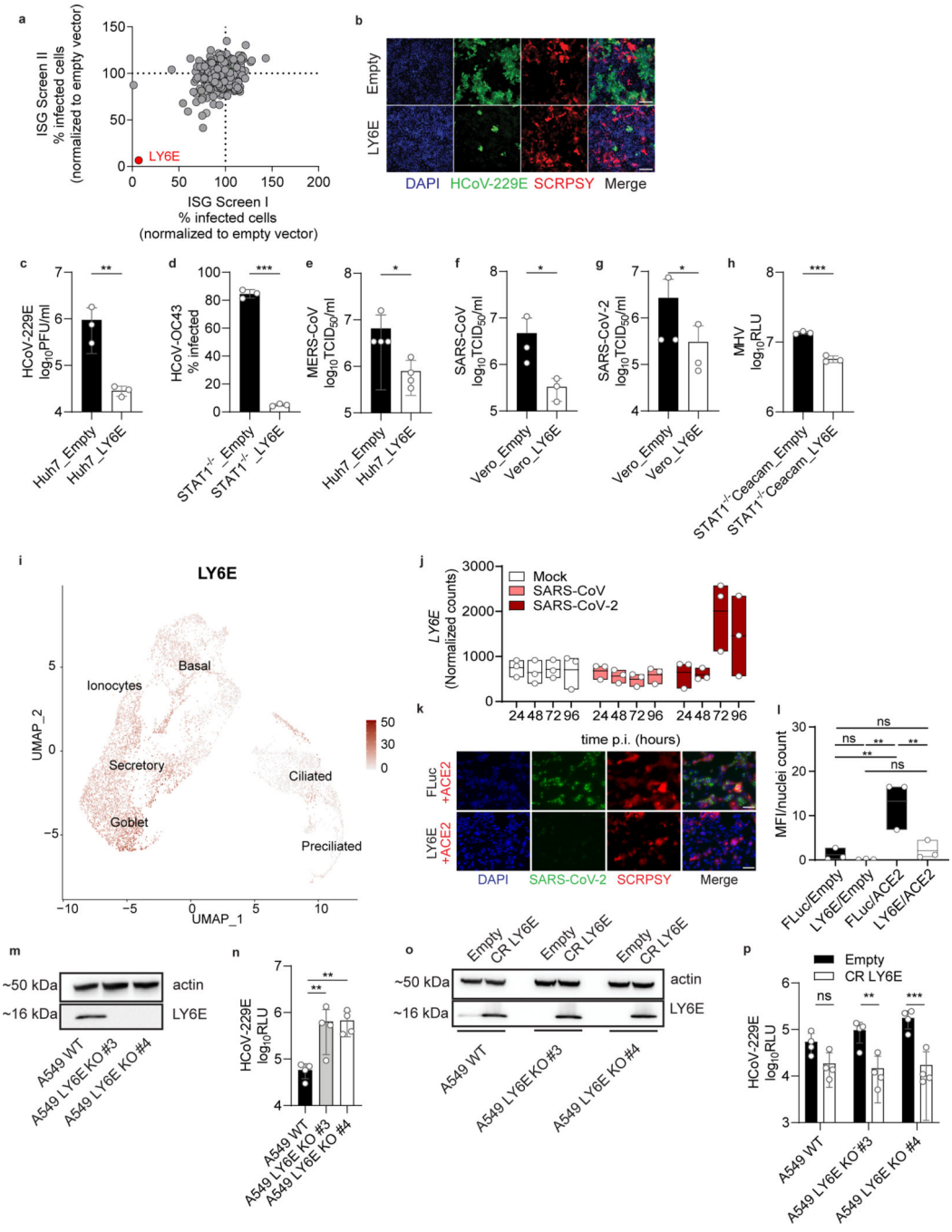

Figure 1. ISG screen identifies LY6E as a potent coronavirus restriction factor.

a, Duplicate screens depicting HCoV-229E infection (24 hours post-infection) in Huh7 cells ectopically expressing ISGs. **b**, HCoV-229E infection of Huh7 cells expressing LY6E or control vector (Empty). Blue: DAPI, green: HCoV-229E N protein, red: TagRFP encoded in SCRPSY vector. **c-h**, Effect of stable LY6E expression on diverse coronaviruses. Cells were infected with HCoV-229E (**c**), HCoV-OC43 (**d**), MERS-CoV (**e**), SARS-CoV (**f**), SARS-CoV-2 (**g**), MHV-Gluc (**h**). **i**, UMAP visualization of *LY6E* expression and distribution in primary hAEC cultures from 2 donors by scRNA-seq. **j**, Induction of *LY6E* in mock or

Author Manuscript Author Manuscript Author Manuscript Author Manuscript

infected hAEC from 3 donors by RNA-seq. **k**, SARS-CoV-2 infection of LY6E or control vector (FLuc) Huh7.5 cells co-expressing human ACE2. Blue: DAPI, green: SARS-CoV-2 dsRNA, red: TagRFP encoded in SCRPSY-ACE2 vector. **l**, Quantification of overall dsRNA fluorescence intensity normalized by number of nuclei in the image. **m**, Western blot of WT A549 or two LY6E KO clones (#3, #4). **n**, HCoV-229E infection of WT or LY6E KO A549. **o**, Western blot of WT or LY6E KO A549 reconstituted with CRISPR-resistant LY6E (CR LY6E) or control vector (Empty). **p**, HCoV-229E infection of CR LY6E-reconstituted WT or LY6E KO A549. Data represent mean of independent biological replicates, n=3 (**c-d,f-h,j,l**), n=4 (**e**,**n,p**). Immunofluorescence images are depicted exemplarily from n=2 (**b**) and n=3 (**k**). In **l,** seven images per condition were acquired and processed. In **b**, scale bars are 200 μM and in **k**, scale bars are 100 μM. Statistical significance was determined by two-tailed unpaired student's t-test with Welch's correction (**c-d**,**f,h**), one-tailed Mann-Whitney U test (**e**), two-tailed ratio paired student's t-test (**g**), one-way ANOVA followed by Tukey's multiple comparisons test (**l**), or two-way ANOVA followed by Sidak's or Dunnett's multiple comparison test (**n,p**). For box plots, center line indicates mean and upper and lower bounds respectively indicate maximum and minimum replicate values (**j**,**l**). Error bars: SD. *P* values: **c**, ** p=0.0088; **d**, *** p=0.0001; **e**, * p=0.0143; **f**, * p=0.0286; **g**, * p=0.0101; **h**, *** p=0.0010; **l**, ** p=0.0035, ** p=0.0091, **p=0.0057; **n**, ** p=0.0073, ** p=0.0033; **p**, ** p=0.0013, *** p=0.0001.

Author Manuscript
Author Manuscript
Author Manuscript
Author Manuscript

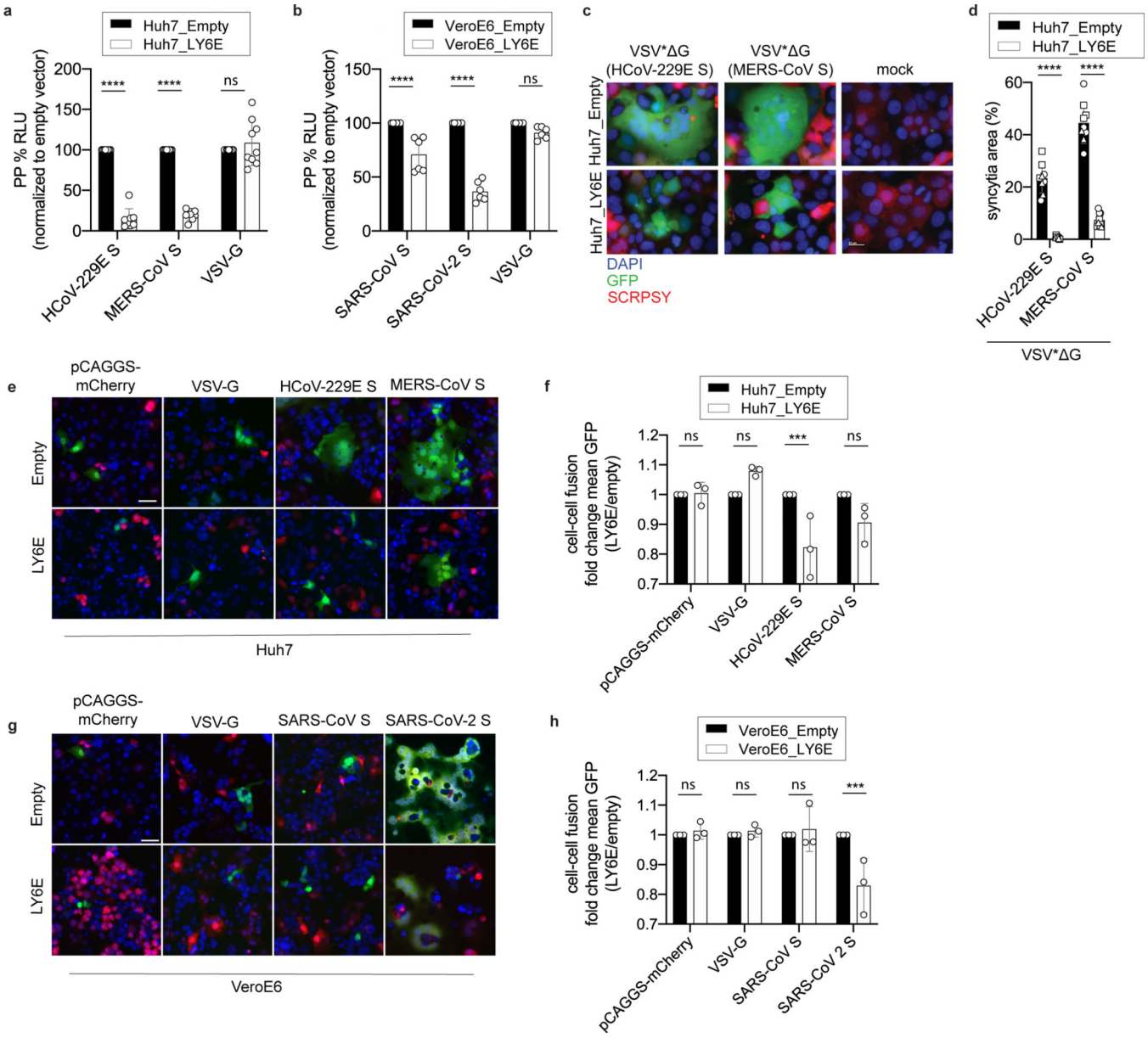

Figure 2. LY6E inhibits viral membrane fusion and syncytia formation.

a-b, VSV pseudoparticles (pp) harboring spike proteins from (**a**) HCoV-229E, MERS-CoV and G protein from VSV or (**b**) SARS-CoV, SARS-CoV-2 and G protein from VSV were inoculated on LY6E- or empty vector-expressing cells. Virus entry efficiency was quantified by measuring virus-encoded luciferase reporter activity. **c**, VSV pp expressing VSV G protein on their surface and encoding CoV S protein and GFP (VSV*ΔG(CoV S)) were inoculated with LY6E- or empty vector-expressing Huh7. Syncytia formation was analyzed by immunofluorescence microscopy. Blue: DAPI, green: GFP, red: TagRFP inserted in SCRPSY vector. **d**, Quantification of VSV*ΔG(CoV S)-induced syncytia depicted as percentage syncytia area. Three independent areas were analyzed per biological replicate (circle, square, triangle). **e-h**, Cell-cell fusion was analyzed by co-incubating cells transfected with plasmids encoding mCherry, VSV-G protein, or CoV S proteins and a split-

Author Manuscript Author Manuscript Author Manuscript Author Manuscript

luciferase/split-GFP construct together with CoV permissive LY6E-expressing or control cells transfected with the complementary fragment of split-luciferase/split-GFP. In **e, g**, GFP complementation was analyzed via immunofluorescence microscopy of GFP-positive syncytia. In **f,h**, four images per condition were acquired and processed. Data were normalized to empty control and are depicted as fold change mean GFP. Data represent mean of independent biological replicates, n=8 (HCoV-229E S, MERS-CoV-S) n=9 (VSV-G) (**a**), n=6 (**b**), n=3 (**d**), n=3 (**f**,**h**). Statistical significance was determined by two-way ANOVA followed by Sidak's multiple comparison test (**a-h**). In **c**, scale bar is 20 μM, in **e, g**, scale bar is 50 μM. Error bars: SD (**a-b**, **d**, **f**, **h**). P values: **a**, **** $p=3.3 \times 10^{-16}$, **** $p=3.6 \times 10^{-15}$; **b**, **** $p=1.363 \times 10^{-6}$; **** $p=4.200 \times 10^{-14}$; **d**, **** $p=6.0 \times 10^{-9}$, $p=<1.1 \times 10^{-15}$; **f**, *** p=0.0008; **h**, *** p=0.0008.

Author Manuscript Author Manuscript Author Manuscript Author Manuscript

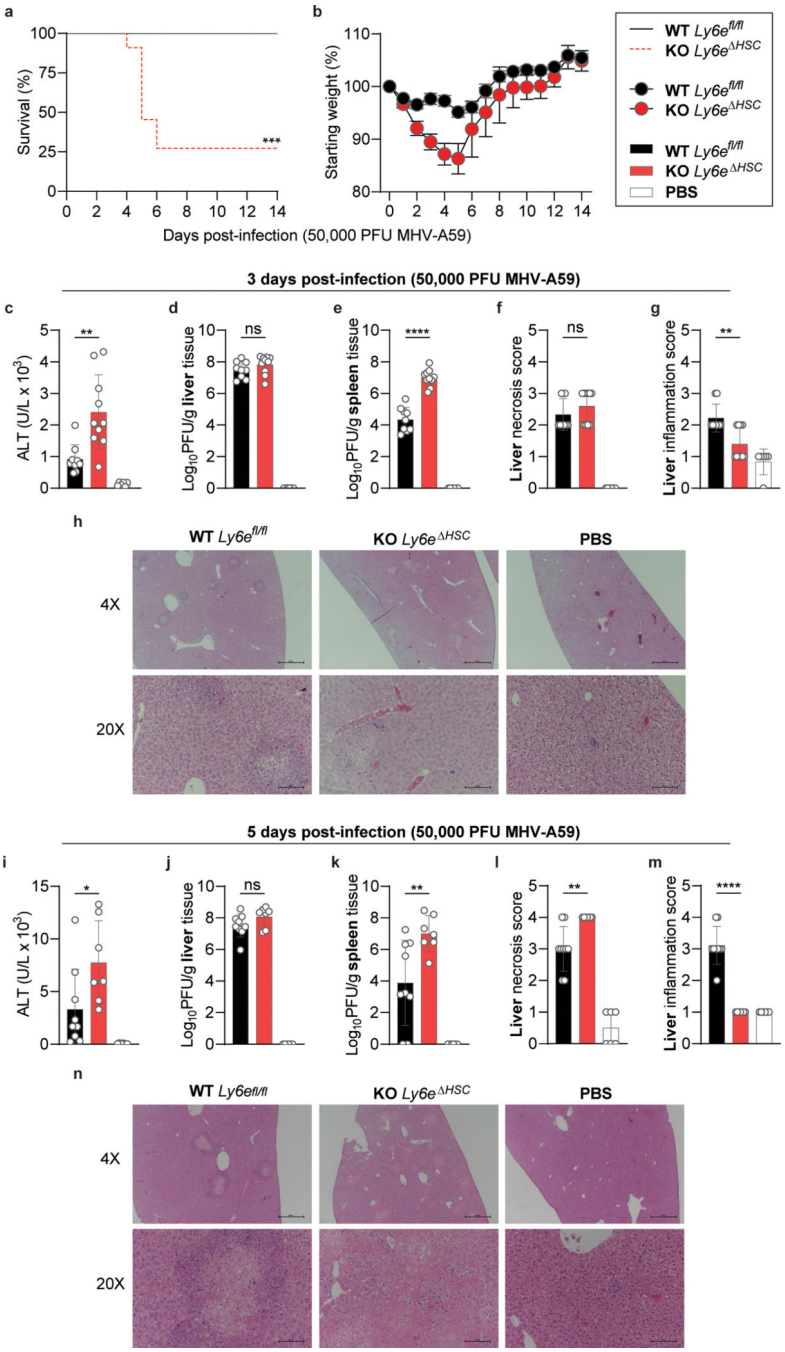

Figure 3. *Ly6e*$^{\Delta HSC}$ mice are more susceptible to mouse hepatitis virus.

a-b, Female *Ly6e*$^{fl/fl}$ and *Ly6e*$^{\Delta HSC}$ mice were injected with PBS or MHV and monitored for survival (**a**) and weight loss (**b**). **c-n**, Mice were assessed at 3 (**c-h**) or 5 (**i-n**) days post-infection for serum ALT (**c,i**), viral titers in liver (**d,j**) and spleen (**e,k**), and liver necrosis and inflammation (**f-h**, **l-n**). For **a-b**, n=13 for days 0–14 (*Ly6e*$^{fl/fl}$), n=11 for day 0–3, n= 10 for days 4–5, n=5 for days 5–6, n=3 for days 6–14 (*Ly6e*$^{\Delta HSC}$) from three pooled experiments. For **c-g**, data represents mean value of n=9 (*Ly6e*$^{fl/fl}$), n=10 (*Ly6e*$^{\Delta HSC}$), n=6 (PBS) from two pooled experiments; images in **h** are representative of the same cohorts. For

Author Manuscript Author Manuscript Author Manuscript Author Manuscript

i-m, data represents mean value of n=9 (*Ly6e*$^{fl/fl}$,), n=7 (*Ly6e*$^{\Delta HSC}$), n=6 (PBS) from two pooled experiments; images in **n** are representative of the same cohorts. In **h,n**, scale bars are 500 μM (4x) and 100 μM (20x). Statistical significance was determined by two-sided Mantel-Cox test (**a**), two-tailed unpaired student's t-test with Welch's correction (**c-e**, **i-k**), two-tailed Mann-Whitney U test (**f-g**, **l-m**). Data are presented as mean values ± SEM (**b**) or SD (**c-g**, **i-m**). *P* values: **a**, *** p=0.0002; c, ** p=0.0031; **e**, **** p=5.759 × 10^{-7}; **g**, ** p=0.0054; **i**, * p=0.0430; **k**, ** p=0.0094; **l**, ** p=0.0072; **m**, **** p=8.741 × 10^{-5}.

Author Manuscript Author Manuscript Author Manuscript Author Manuscript

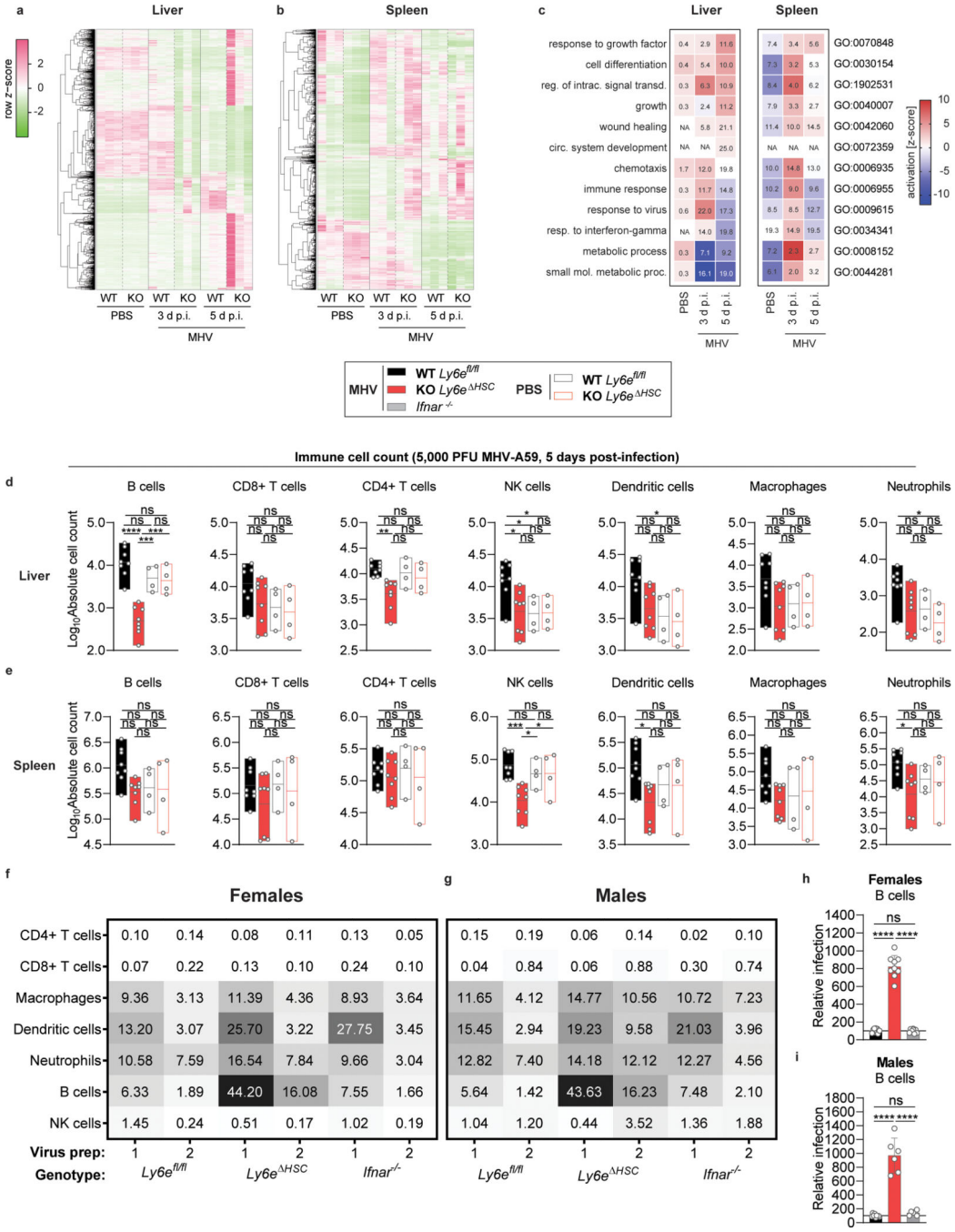

Figure 4. Hematopoietic Ly6e protects against mouse hepatitis virus-induced alterations in liver and spleen.

a-c, Transcriptomic analyses from female *Ly6e*$^{fl/fl}$ (WT) and *Ly6e*$^{\Delta HSC}$ (KO) mice. **a-b**, Heat maps displaying significant changes (mean RPKM > 0.5; fold change > 2; FDR ≤ 0.05) in liver (**a**) and spleen (**b**). Dendrograms are normalized read data (row z-score) clustered with complete linkage method employing Spearman Rank correlation distance measurement. **c**, Pathway analysis of KO versus WT. Up- (red) or down-regulated (blue) pathways indicated by activation z-score. Numbers show significantly dysregulated genes as

Author Manuscript Author Manuscript Author Manuscript Author Manuscript

percentage of total gene number included in pathway. **d-e**, Immune cell counts from liver (**d**) and spleen (**e**) of female mice. **f-g**, Heatmap of average MHV-GFP infectivity of cultured splenocytes from female (**f**) and male (**g**) mice with two independent viral preparations. **h-i**, MHV-GFP infection of splenic B cells from females (**h**) and males (**i**) normalized to average (line at 100) of *Ly6e*$^{fl/fl}$ mice. For **a-c**, n=3. For **d-e**, n=8 MHV-injected, n=4 PBS-injected from two pooled experiments. For **f,h**, n=9 (*Ly6e*$^{fl/fl}$ and *Ly6e*$^{\Delta HSC}$) and n=8 (*Ifnar*$^{-/-}$) from four pooled experiments. For **g**,**i**, n=9 (*Ly6e*$^{fl/fl}$), n=6 (*Ly6e*$^{\Delta HSC}$), and n=6 (*Ifnar*$^{-/-}$). Significance for **d-e, h-i** was determined by one-way ANOVA with Tukey's multiple comparisons test. For box plots, center line indicates mean and upper and lower bounds respectively indicate maximum and minimum replicate values (**d-e**). Error bars: SD (**h-i**). *P* values (top-bottom, then left-right): **d**, **** $p=4.242 \times 10^{-7}$, *** $p=8.902 \times 10^{-4}$, *** $p=4.581 \times 10^{-4}$; ** p=0.0030; * p=0.0436, * p=0.0381, * p=0.0148; * p=0.237; * p=0.0173; **e**,*** $p=8.395 \times 10^{-4}$, * p=0.0414, * p=0.0439; * p=0.0233; * p=0.0295; **h**, **** $p=1.1 \times 10^{-14}$, **** $p=1.2 \times 10^{-14}$. **i**, **** $p=1.1416 \times 10^{-9}$, **** $p=1.0469 \times 10^{-8}$.